

A Numerical Study of Dynamic Capillary Pressure Effect for Supercritical Carbon Dioxide-Water Flow in Porous Domain

Diganta B. Das[#], Bhupinder S. Gill, Luqman K. Abidoye, Kamal Khudaida

Department of Chemical Engineering, Loughborough University, Loughborough LE11 3TU, Leicestershire

[#]Corresponding Author (Email: d.b.das@lboro.ac.uk)

Abstract

Numerical simulations for core-scale capillary pressure (P^c)–saturation (S) relationships have been conducted for a supercritical carbon dioxide-water system at temperatures between 35°C and 65°C at a domain pressure of 15 MPa as typically expected during geological sequestration of CO₂. As the P^c -S relationships depend on both S and time derivative of saturation ($\partial S/\partial t$) yielding what is known as the ‘dynamic capillary pressure effect’ or simply ‘dynamic effect’, this work specifically attempts to determine the significance of these effects for supercritical carbon dioxide-water flow in terms of a coefficient, namely dynamic coefficient (τ). The coefficient establishes the speed at which capillary equilibrium for supercritical CO₂-water flow is reached. The simulations in this work involved the solution of the extended version of Darcy’s law which represents the momentum balance for individual fluid phases in the system, the continuity equation for fluid mass balance, as well as additional correlations for determining the capillary pressure as a function of saturation, and the physical properties of the fluids as a function of temperature. The simulations were carried out for 3D cylindrical porous domains measuring 10 cm in diameter and 12 cm in height. τ was determined by measuring the slope of a best-fit straight line plotted between (i) the differences in dynamic and equilibrium capillary pressures ($P^{c,dyn} - P^{c,equ}$) against (ii) the time derivative of saturation (dS/dt), both at the same saturation value. The results show rising trends for τ as the saturation values reduce, with noticeable impacts of temperature at 50% saturation of aqueous phase. This means that the time to attain capillary equilibrium for the CO₂-water system increases as the saturation decreases. From a practical point view, it implies that the time to capillary equilibrium during geological sequestration of CO₂ is an important factor and should be accounted for while simulating the flow processes, e.g., to determine the CO₂ storage capacity of a geological aquifer. In this task, one would require both the fundamental understanding of the dynamic capillary pressure effects for supercritical CO₂-water flow as well as τ values. These issues are addressed in this paper.

Keywords: Two-phase flow, geological sequestration, capillary pressure, dynamic coefficient, porous media

1. Introduction

Technologies for carbon dioxide storage into subsurface formations are widely regarded as one of the most viable options to help reduce the amount of carbon dioxide (CO₂) in the atmosphere and its adverse effects. Typically, CO₂ is injected into deep geological formations in a supercritical (sc) state. In this process, the temperatures and pressures within these formations would still be sufficient for the injected CO₂ to exist in its supercritical state (Doughty and Pruess, 2003; Khudaida and Das, 2014). Under such conditions, the density of the supercritical fluid is significantly higher than that of gaseous CO₂ but, in most circumstances, lower than that of the resident formation water or brine. Likewise, the viscosity of the supercritical CO₂ (scCO₂) is lower than that of water/brine.

A vast amount of research has been conducted on carbon capture and subsurface injection processes as indicated by many reviews on the subject (e.g., Stanmore and Gilot, 2005; Abu-Khader, 2006; Zakkour et al., 2007; Tsang et al., 2008; Huh et al., 2009; Daneshfar et al., 2009; Michael et al., 2010; Shukla et al., 2010; Müller, 2011; Zahid et al., 2011; Abidoye et al., 2014) which also reference a large number of other research publications. It is obvious from these literatures that computational methods have been widely used for resolving questions associated with the injection of CO₂ into deep geological formations. These computational techniques are applied to address issues related to the site characterisation and monitoring and, making assessments of potential leakage. Specifically for models on supercritical CO₂ flow and transport in these media, it is clear that two approaches are most commonly used in these studies. In the first approach, the authors apply models of convection-diffusion-dissolution processes (e.g., Ennis-King and Paterson, 2003; Riaz et al., 2006; Pruess and Zhang, 2008). The CO₂-rich fluid resulting from the dissolution of CO₂ into brine at the interface of the CO₂-brine system after CO₂ injection is defined to be slightly denser than the surrounding brine causing negative buoyancy. This increase in density causes downward movement of the CO₂-rich fluid towards the bottom of the aquifer. Convective mixing may be considered in these models as it promotes the dissolution of CO₂ into the brine (Ozgun and Gumrah, 2009). However, this approach does not consider the concept of fine scale capillary pressure in the porous media (e.g., see, Pruess and Zhang, 2008).

In the second approach, the supercritical CO₂ and water/brine are defined to behave as two immiscible fluid phases, particularly at very early period of injection and displacement in the aquifer. They are therefore described by capillary pressure-saturation (P^c-S) relationships along with relative permeability-saturation (K_r-S) functions (e.g., Plug and Bruining, 2007; Perrin et al., 2009; Lopez et al., 2011; Khudaida and Das, 2014).

This paper does not use the first approach of convection-diffusion-dissolution and is concerned with the second modelling approach. The second approach applies the extended version of Darcy's law for

multiphase flow together with the constitutive relationship for capillary pressure as a function of saturation as in equation (1).

$$P_{nw} - P_w = P^{c,eq} (S) = f(S) \quad (1)$$

where,

P_{nw} = average pressure for non – wetting phase [$ML^{-1}T^{-2}$]

P_w = average pressure for wetting phase [$ML^{-1}T^{-2}$]

S = wetting phase saturation [-]

$P^{c,eq}$ = equilibrium (steady state) capillary pressure [$ML^{-1}T^{-2}$]

Traditionally, equation (1) is defined to include the effects of all factors that determine equilibrium saturation distribution of fluids in porous domains. However, the P^c - S relationship (equation (1)) has been shown to depend on both S and $\partial S/\partial t$ in a number of studies (Topp et al., 1967; Kalaydjian 1992; Bottero et al., 2011a,b; Camps-Roach et al., 2010; Das and Mirzaei, 2012; Das and Mirzaei 2013). This dependence is known as the ‘dynamic capillary pressure effect’ or simply ‘dynamic effect’. In the publications on multiphase flow in porous media, there have been significant amounts of discussions on the role of dynamic capillary pressure where it has been shown that the definition of P^c may suffer setback owing to its inability to address the dynamic characteristics of the capillary pressure prior to attainment of capillary equilibrium (e.g., Gray and Hassanizadeh, 1990, 1993; Sakaki et al., 2010; Das and Mirzaei, 2012, Das and Mirzaei, 2013). The need for modification of the traditional capillary pressure relation was the conclusion of many authors. This was suggested to accommodate a more complete description of the capillary pressure (Hassanizadeh and Gray, 1990; 1993) with the inclusion of a phenomenal factor, namely, a dynamic coefficient (τ) (e.g., Hanspal et al., 2013; Das and Mirzaei, 2012, 2013; Hanspal and Das, 2012; Bottero et al., 2011a,b; Camps-Roach et al., 2010; Das et al., 2007, Mirzaei and Das, 2007; Dahle et al., 2005; Hassanizadeh et al., 2002). The modification to equation (1) is mathematically expressed in equation (2):

$$(P^{c,dyn} - P^{c,eq})|_s = -\tau \partial S/\partial t|_s \quad (2)$$

where,

$P^{c,dyn}$ \equiv dynamic capillary pressure [$ML^{-1}T^{-2}$]

$P^{c,eq}$ \equiv equilibrium (steady state)capillary pressure [$ML^{-1}T^{-2}$]

$\partial S/\partial t$ \equiv time derivative of saturation [T^{-1}]

τ \equiv dynamic coefficient [$ML^{-1}T^{-1}$]

The physical interpretation of $P^{c,dyn}$ and $P^{c,eq}$ together with the difference between them have been discussed previously extensively (e.g., Hassanizadeh et al., 2002; Bottero et al., 2011a,b; Das and Mirzaei, 2012, 2013). The slope of the linear relationship between $(P^{c,dyn} - P^{c,eq})$ and $\partial S/\partial t$ in

equation (2) is the dynamic coefficient (τ) and it provides a quantitative basis for determining the significance of the dynamic capillary pressure effect. For example, if τ is small, the equivalence between $P^{c,dyn}$ and $P^{c,equ}$ is established quickly, and/or vice versa. In the context of dynamic capillary pressure effect, the determination of τ values may be viewed as an ‘inverse approach’ where all other quantities are assumed known except the values of the dynamic coefficient. Once the significance of its values is understood, a ‘forward problem’ for simulating the dynamic two-phase flow processes which couples equation (2) may be set up, e.g., please see the papers by Fučík et al (2010) and Peszyńska and Yi (2009).

It seems that although there are no significant inconsistencies in the definitions of equilibrium capillary pressure, $P^{c,equ}$, the interpretation of $P^{c,dyn}$ may vary. For example, Bottero et al. (2011a) argue that $P^{c,dyn}$ should be viewed as an ‘apparent’ capillary pressure. We maintain continuity from our previous work (Mirzaei and Das, 2007; Das et al., 2007; Hanspal and Das, 2012; Hanspal et al., 2012; Das and Mirzaei, 2012, 2013) and use the dynamic capillary pressure (when $\partial S/\partial t$ is non-zero) in order to describe $P^{c,dyn}$. There is now a good amount of literatures on simulation and experimental works performed to explore the significance of τ in a number of circumstances involving two-phase flow process, as well as to explore its range of values and a number of factors have subsequently been reported to have effects on values of τ . Some of these include, e.g., permeability anisotropy and media heterogeneities (Manthey et al., 2005; Mirzaei and Das, 2007), temperature (Hanspal and Das, 2012; Civan, 2012), fluid properties (Das et al., 2007; Goal and O’Carroll, 2011) and porous media mean grain size (Camps Roach et al., 2010; Das and Mirzaei, 2012, 2013).

In a number of recent papers on dynamic capillary pressure effect, geological sequestration of CO_2 has been used as an example of multiphase flow in porous media (e.g., Juanes, 2008; Camps Roach et al., 2010; Goel and O’Carroll, 2011; Khudaida and Das, 2014). These papers suggest that dynamic capillary pressure effect is an important consideration of the in-situ conditions of the geological formation for CO_2 sequestration despite the fact that fluid flow or saturation change may occur slowly. This is similar to other processes in the subsurface (e.g., oil extraction) where fluid flow velocity may be slow but the dynamic capillary pressure effect has been shown to be important. Dynamic effect is defined to be the dependence of $P^{c,dyn} - P^{c,equ}$ on $\partial S/\partial t$ as shown in equation (1), and is not directly related to the flow velocity of the fluid phases. As such, it is not clear how significant the dynamic capillary pressure effect is in the context of this paper. Furthermore, it seems that there is no work currently in the literature specifically for the dynamic capillary pressure effects in the $scCO_2$ -water system.

From the above discussion it is clear that a number of questions have remained unaddressed, e.g., is the dynamic capillary pressure effect really significant in $scCO_2$ -water flow in porous media and if so

how can the dynamic coefficient be calculated in this case, what is its range of values and how does it compare with the values reported in the literature for other two-phase system? Indeed there is no work at the moment that shows the quantitative significance of the dynamic capillary pressure effect for scCO₂-water flow in any kind of porous media in general and, geological sequestration of CO₂, in specific. Since geological sequestration of CO₂ takes place at much higher temperature and pressure as compared to other typical laboratory studies on dynamic capillary pressure effect (e.g., Camps Roach et al., 2010; Bottero et al., 2011a,b; Das and Mirzaei, 2012; Mirzaei and Das, 2013), it is also uncertain if any of the reported values of the dynamic coefficient would represent the significance of dynamic effect in the case of CO₂ sequestration. This paper aims to address these knowledge gaps by determining the dynamic capillary pressure effect (dynamic coefficient) for supercritical CO₂-water flow in porous media. In particular we aim to carry out simulations for core scale porous domain where the porous materials are unconsolidated (discussed further in the next section). The numerical simulations are needed as they help determine the significance of the dynamic effects and direct future experiments and simulations for different porous media properties (e.g., heterogeneous domains, ultra-low or ultra-high permeability domains, larger or smaller domain).

In order to achieve these aims, numerical simulations are conducted for homogeneous domains of laboratory scale. The simulations are carried out for a 3D cylindrical domain measuring 10 cm in diameter and 12 cm in height with a view to determine the dynamic capillary pressure effects indicated by a dynamic coefficient (τ). The geological formations can have varying temperatures depending on their respective geothermal gradients (G) and average land surface temperatures. Therefore, the temperature effects on the dynamic coefficient are accounted for with inclusion of other physical effects such as temperature dependent properties of the two-phase system. In order to obtain correlated material properties for the simulations, well defined core samples (column) of sand particles of known particle size range are prepared and the corresponding properties (e.g., porosity and intrinsic permeability) are determined experimentally. The capillary pressure-saturation curves at equilibrium and dynamic conditions as well as dynamic coefficients were then determined numerically as described in the following sections. Furthermore, the detailed procedures for the numerical simulations including the details of the method are described in the next section.

2. Modelling Strategy

In the context of this paper, modelling the two-phase flow processes involves the solution of the conservation laws for fluid mass and momentum while taking into account the relevant P^c-S-K_r relationships at different temperatures. In specific, this involves the solution of the extended version of Darcy's law which represents the momentum balance for individual fluid phases in the system. It also involves the solution of the continuity equation as a statement of the fluid mass balance as well as additional models for determining the capillary pressure as a function of saturation, and the physical properties of the fluids as a function of temperature. In order to characterise the dynamics of the

system, the dynamic coefficient is determined by measuring the slope of the line corresponding to values of $(P^{c,dyn} - P^{c,eq})$ against $\partial S/\partial t$ from equation (2).

2.1 Governing Model Equations for Two-Phase Flow in Porous Media

The numerical simulations in this work are designed to mimic the pressure cell type of experiments which are typically used to determine the P^c - S curves in laboratory conditions. In this type of experiments, the top and bottom boundaries are permeable to only one of the fluid phases. Such flow cells have been used by several previous authors (e.g., Plug and Bruining, 2007; Das and Mirzaei, 2012, 2013). The two-phase flow behaviour in this pressure cell is simulated as follows.

As shown in equation (3), an extended version of Darcy's law is used as the governing conservation equation of motion for both the wetting (w) and non-wetting phases (nw):

$$q_\gamma + \frac{K_{r\gamma}k}{\mu_\gamma} \cdot \nabla P_\gamma = 0 \quad \text{for } \gamma \equiv w, nw \quad (3)$$

where,

$q \equiv$ fluid flow velocity [LT^{-1}]

$K_r \equiv$ relative permeability [-]

$k \equiv$ intrinsic permeability tensor [L^2]

$\mu \equiv$ viscosity [$ML^{-1}T^{-1}$]

$P \equiv$ average pore pressure [$ML^{-1}T^{-2}$]

The conservation of mass for the wetting (w) and non-wetting (nw) phases is described with equation (4).

$$\frac{\partial}{\partial t}(\emptyset \rho_\gamma S_\gamma) + \nabla \cdot (\rho_\gamma q_\gamma) = 0 \quad \text{for } \gamma \equiv w, nw \quad (4)$$

where,

$\emptyset \equiv$ porosity of the medium [-]

$\rho \equiv$ fluid density [ML^{-3}]

$S \equiv$ average fluid saturation [-]

The Brooks-Corey formulations, as shown in equations (5)-(7), are used as the governing equations for capillary pressure-saturation relationships (Brooks and Corey, 1964).

$$S_w = \left(\frac{P^c}{P^d}\right)^{-\lambda} \quad \text{for } P^c \geq P^d \quad (5)$$

$$S_{ew} = 1 \quad \text{for } P^c \leq P^d \quad (6)$$

$$S_{ew} = \left(\frac{S_w - S_{rw}}{1 - S_{rw}} \right) \text{ for } 0 \leq S_{ew} \leq 1 \quad (7)$$

where,

$S_{ew} \equiv$ effective saturation of the wetting phase [–]

$P^d \equiv$ entry pressure for non – wetting phase [$ML^{-1}T^{-2}$]

$\lambda \equiv$ pore size distribution index [–]

$S_{rw} \equiv$ irreducible wetting phase saturation [–]

The Brooks-Corey-Burdine formulae (Brooks and Corey, 1964) were employed for relative permeabilities (K_r) of the porous media to the wetting and non-wetting phases:

$$K_{rw} = S_{ew}^{(2+\lambda)/\lambda} \quad (8)$$

$$K_{rnw} = (1 - S_{ew})^2 \left(1 - S_{ew}^{\frac{2+\lambda}{\lambda}} \right) \quad (9)$$

The numerical simulator, STOMP (Subsurface Transport Over Multiple Phases), was used for conducting the modelling exercises. STOMP is a computer model developed by the hydrology group at the Pacific Northwest National Laboratory (White and Oostrom, 2006). It has abilities that allow the user to specify and manipulate capillary pressure-saturation-relative permeability (P^c - S - K_r) relationships via a variety of functions, making it ideal for describing fundamental two-phase flow mechanisms. While using STOMP, the user can choose the governing equations for the modelling purpose. In the case of our work, we have used STOMP to solve equations (3) – (9). The code uses the finite volume method (FVM) to discretise the partial differential equations (equations (3) and (4)) into the non-linear algebraic equations, and Euler-backward time differencing for spatial and temporal discretizations, respectively. The produced algebraic equations in the discretised equations are closed using a number of constitutive relationships (equations (5) to (9)) and solved using the Newton-Raphson iteration to resolve their nonlinearities (White and Oostrom, 2006).

2.2 Selection of Simulation Conditions

It is important to define the temperatures and pressures at which sequestration occurs in order to accurately determine the densities and viscosities of carbon dioxide and water under such conditions. This is mainly because buoyancy forces and mobility ratio between the two fluid phases tend to differ depending on the physical conditions, thus affecting the dynamic flow mechanisms. Nordbotten et al. (2004) class sedimentary basins according to geothermal regimes. These basins have been classified as “warm” or “cold” depending on their respective geothermal gradients (G) and average land surface temperatures. Warm basins have G values of around $45^{\circ}C/km$ with a surface temperature of around $20^{\circ}C$. On the other hand, cold basins have G values of around $25^{\circ}C/km$ with a

surface temperature of around 10°C. CO₂ storage ideally takes place at depths below 800 m. The depths at which injection occurs can be classified as “shallow” for depths up to 1000 m, or “deep” at depths of around 3000 m. An injection depth of 1000 m was assumed for the purpose of this paper, which equates to temperatures ranging between 35°C for “cold” basins and 65°C for “warm” basins.

Birkholzer et al. (2009) measured a pressure gradient of around 0.181 bar/m in saline aquifers, which equates to a pressure of 18 MPa at a depth of 1000 m. This pressure gradient can vary depending on the compositions and structures of the sedimentary rocks. Additionally, in a recent paper by Benson et al. (2011), sequestration experiments and simulations were conducted at pressures of around 12 MPa. A domain pressure of 15 MPa was selected for this study.

The critical temperature and pressure of carbon dioxide are 31.1°C and 7.382 MPa, respectively, above which it exists as a supercritical fluid. In all our simulations, temperatures were varied between 35°C and 65°C while maintaining the domain pressure (15MPa). Under such conditions, the carbon dioxide would remain in a supercritical state. Furthermore, the simulations were carried out for the case when the geological formation contains water and not brine.

2.2.1 Temperature Dependent Density and Viscosity of Water and Supercritical Carbon Dioxide

The densities of supercritical carbon dioxide and pure water at the conditions selected for the simulations are summarised in Table 1. The carbon dioxide densities were obtained by interpolating experimental results reported by Chiquet et al. (2007). Water densities were calculated as shown in equations (10) – (14):

$$\rho_1 = v_V^{w-1} \{ A_{11} a_5 Z^{-5/17} + A_{12} + A_{13} T_r^w + A_{14} (T_r^w)^2 + A_{15} (a_6 - T_r^w)^{10} + A_{16} (a_7 + (T_r^w)^{19})^{-1} - (a_8 + (T_r^w)^{11})^{-1} (A_{17} + 2A_{18} P_r^w + 3A_{19} (P_r^w)^2 - A_{20} (T_r^w)^{18} (a_9 + (T_r^w)^2 (-3(a_{10} + P_r^w)^{-4} + a_{11})) 3A_{21} (a_{12} - T_r^w) (P_r^w)^2 + 4A_{22} (T_r^w)^{-20} (P_r^w)^3 \}^{-1} \quad (10)$$

$$P_r^w = P / P_c^w \quad (11)$$

$$T_r^w = T / T_c^w \quad (12)$$

$$Y = 1 - a_1 (T_r^w)^2 - a_2 (T_r^w)^{-6} \quad (13)$$

$$Z = Y + (a_3 Y^2 - 2a_4 (T_r^w) + 2a_5 P_r^w)^{1/2}. \quad (14)$$

Where $A_{11} \dots A_{22}$ and $a_5 \dots a_{12}$ are liquid water primary constants, P and T are the water pressures and temperatures respectively, P_c^w and T_c^w are the critical water pressures and temperatures. Values for the constants are given under liquid water constants in Table 2.

As expected, Table 1 shows that as the temperature is increased, the densities of both carbon dioxide and brine decrease. Furthermore, the rate at which the carbon dioxide densities decrease is much greater than that for water. Table 3 summarises the viscosities of carbon dioxide and pure water. Carbon dioxide viscosities were obtained by interpolating experimental results reported by Fenghour et al. (1998). Water viscosities as a function of temperature were calculated using equation (15).

$$\mu_l = \exp(-24.71 + 4209/T + 0.04527T - 3.376 \times 10^{-5}T^2) \quad (15)$$

where,

$\mu_l \equiv$ liquid water viscosity [Pa. s]

$T \equiv$ temperature [K]

The table shows that as temperature is increased, the viscosities of both carbon dioxide and brine decrease. The density and viscosity values as determined above were supplied for the simulations.

We appreciate that there are other approaches which may be used to determine the temperature dependency of liquid properties. For example, Civan (2007) has reported a modification to the Vogel-Tammann-Fulcher (VTF) equation for calculating temperature effects on water density. These approaches may require lesser number of coefficients and exponents in the correlations in comparison to equations (10) – (15). Therefore, the alternative approaches may be attractive in some cases. The equations we have used (equations (10)-(14)) in this work represent the data in steam tables (Meyer et al., 1967) and are well recognised. These equations also maintain continuity from our previous work (Hanspal and Das, 2012). For these reasons, we have used the equations mentioned in this section and not an approach such as the one reported by Civan (2007).

2.2.2 Interfacial Tensions

Interfacial tensions affect P^c-S relationships in two-phase flow behaviour. Thus, the simulator also required us to specify carbon dioxide-water and water-air interfacial tensions under the various simulation conditions. Carbon dioxide-water interfacial tensions at 15 MPa between 35^oC and 65^oC were obtained using experimental results reported by Bachu and Bennion (2009). Water-air interfacial tensions were calculated using equation (16).

$$\gamma^{lg} = a_0^{lg} + a_1^{lg}T \ln(T) + c^{lg}T \quad (16)$$

where,

$\gamma^{lg} \equiv$ water – air interfacial tension [Nm⁻¹]

constants a_0^{lg} , a_1^{lg} and $c^{lg} = 67.82, -0.16889, \text{ and } 0.9766$ respectively [dyn cm⁻¹K⁻¹]

$T \equiv$ temperature [K]

Values for the interfacial tensions are presented in Table 4.

2.2.3 Irreducible Saturation

Increasing temperature causes the irreducible water saturation in the porous media to increase. Equation (17) was used to account for the effects of temperature on irreducible saturation, S_{rw} with the calculated values presented in Table 5:

$$S_{rw} = a_r + b_r T \quad (17)$$

where,

constants a_r and $b_r \equiv -1.274$ and 0.00438 , respectively [-]

$T \equiv$ temperature [K]

The table shows that at 35⁰C, if the porous sample is initially fully saturated with water, it is theoretically possible to displace approximately 93% of the water with carbon dioxide using capillary forces. As the temperature is increased to 65⁰C, only 79% of the water can be displaced. Therefore, selecting injection sites in high temperature sedimentary basins could cause significant reduction in storage capacities.

2.3 Description of Porous Media Properties for Simulations

For the purpose of this paper, various properties of fine and coarse grained sand were determined experimentally for core samples. This was done with a view to utilizing realistic sample properties for the simulations as well as to relate the particle size to the dynamic effect in capillary pressure relationship for CO₂ injection as done previously for other fluid systems (e.g., Camps-Roach et al. 2010; Das and Mirzaei, 2012, 2013). The porous media samples are silica sand (quartz) with coarse grained sample (DA 14/25) and fine grained sample (CH30) which were purchased from Minerals Marketing Ltd, Nantwich Cheshire, UK. The particle densities were determined using a Helium Pycnometer (Micromeritics Model 1305, Norcross, U.S.A.) while the intrinsic permeabilities were determined using a constant head permeameter. Physical properties of a mixture consisting 50% fine grained sand and 50% coarse grained sand were also determined and used in our simulations. All simulations were based on a porous domain on a core-scale which is homogeneous in terms of porosity and intrinsic permeability. Measured properties of the porous samples are summarised in Table 6.

The porous samples chosen for this paper are chosen for unconsolidated laboratory scale porous samples where the correlation between particle size, porosity, permeability and level of compaction can be maintained. In a similar approach, Plug and Bruining (2007) have used porous domains for studying supercritical CO₂ injection which have porosities (0.37-0.38) like our domains and permeability of $k \sim 2 \times 10^{-10} \text{ m}^2$, which is larger than our fine grained sand permeability and almost the

same as our coarse grained sand permeability. The main reason for choosing these porous samples is that we wanted to avoid using uncorrelated parameter values (e.g., particle size, porosity, permeability, Brooks-Corey parameters) because a number of papers (including some of our own) relating to the dynamic effect show that there is an interplay of variables which affect the dynamic coefficient. By choosing the correlated medium parameters, we ensure that correct lumped effects of the material parameters on the dynamic coefficient accounted for. Furthermore, this approach allows us to place the significance of the dynamic effect for CO₂-water system in the context of other studies on dynamic capillary pressure effect (e.g., silicone oil-water flow in porous media) which have used porous domains of similar properties. As shown in this paper, the paper does suggest that the dynamic effect could be important for supercritical CO₂-water flow in porous media and so it should direct further work, e.g., design of future laboratory experiments. We appreciate that in the field scale the porous medium properties may vary (e.g., Daneshfar et al., 2009). However, for the purpose of this paper, which deals with core scale domains, this variability is ignored and we use porous domains where the average permeability is constant in all directions. This is done in an attempt to determine the presence of dynamic capillary pressure effect for CO₂-water flow in porous medium in absence of any other factors.

2.4 Domain Geometry

A 3-dimensional cylindrical domain was chosen with the following geometry. It had a diameter of 10 cm and a vertical length of 12 cm. In Table 7, N represents the number of nodes, Δr is the node spacing in r -direction, $\Delta\Theta$ is the node spacing in Θ direction, and ΔZ is the node spacing in the Z -direction. The chosen cylindrical grid is composed of 416 nodes.

2.5 Initial and Boundary Conditions for Simulations

In all simulations, the conditions were set such that the porous domain was initially fully saturated with water (wetting phase). In order to simulate the dynamic two-phase flow behaviour, the carbon dioxide (non-wetting phase) was introduced through the top of the domain at a constant pressure until the domain attained irreducible wetting phase saturation.

The conditions were set such that there was no out-flow of water through the top of the domain. Neither carbon dioxide nor water could flow out of the domain through the sides. Additionally, only water could flow out via the bottom boundary of the domain. In all simulations, the porous media were assumed to possess homogeneity in bulk properties (e.g., porosity and permeability).

A total of four sets of dynamic simulations were conducted for each of the three porous samples at 35°C, 45°C, 55°C and 65°C. The series of simulations at each temperature were conducted by successively increasing the carbon dioxide pressure head, i.e., simulation 1 at 50 cm head, simulation 2 at 70 cm head, simulation 3 at 100 cm head and simulation 4 at 135 cm head. At each dynamic

condition, the pressure, as CO₂ head, was imposed at once and the water drainage was allowed to continue till irreducible saturation was attained.

Table 8 summarises the boundary conditions for the dynamic simulations conducted in this work. The initial and bottom water pressures in the domain were calculated by taking into account the domain pressure of 15 MPa, water densities and gravity effects. CO₂ pressures, as heads of CO₂ above the domain, were calculated in a similar way but carbon dioxide densities were taken into account instead.

In order to calculate the dynamic coefficient, one quasi-static simulation was conducted for each of the porous samples at the corresponding temperatures. In the quasi-static simulations, the initial and bottom water pressures were kept constant at each of the temperatures shown in Table 8. For the quasi-static process, rather than introducing the carbon dioxide at a single constant pressure, the conditions were set such that pressure was successively increased at various steps within each simulation period. Starting from an arbitrary but very small initial pressure, gradual step increase in pressure followed. At the entry pressure, P^d of the domain, the supercritical CO₂ entered and the water displacement began. This continued until the irreducible saturation was attained. This depends on the imposed tolerance limit. In this work, the limit is reached when saturation at all grid points remains unchanged or desaturation rate ($\partial S/\partial t$) is less than tolerance limit of 10^{-10} .

Each calculated average P^c - S_w point at a particular time for the domain provides a point in the P^c - S_w curve. It corresponds to the wetting phase saturation value, S_w , at which a particular capillary pressure, P^c , is generated in the domain. For the system under quasi-static condition, this is the point where fluid phases move to equilibrium positions such that the imposed forces are the same as forces within the domain (Das et al., 2007). Upon further imposition of pressure on the supercritical CO₂, the displacement continues and drives the system to a new state of equilibrium when the governing forces are once more balanced. This provides a second point on the curve and the procedure follows the same pattern until the 135 cm head is reached which is believed to correspond to condition for irreducible saturation.

During the course of this work, we had tried two approaches for averaging the capillary pressure. The first one is the approach of using an arithmetic mean of the data and the second one involved using saturation weighted average of capillary pressure as discussed by some of our previous paper (Mirzaei and Das, 2007; Hanspal and Das, 2012; Das and Mirzaei, 2012). Both the averaging approaches produced similar results in this work. However, at high water saturation, we observed that the results from the saturation weighted averaging method were slightly more fluctuating than the results from the arithmetic mean. For this reason, we have used the arithmetic averaging method in this paper. We are aware that Nordbotten et al (2007, 2008, 2010) have discussed alternative ways of

averaging capillary pressure and relative permeability data; however, they were not attempted in this paper.

2.6 Determination of Dynamic Coefficient (τ)

The P^c - S curves obtained for the dynamic and quasi simulations from the above procedures were used in determining τ for the domain. For the boundary conditions, respective $P^{c,dyn} - P^{c,eq}$ was plotted against $-\partial S/\partial t$ at the same wetting phase saturation. The plots were fitted to a straight line, the slope of which gives the dynamic coefficient. This is in accordance with Eq. (2) which shows that if $P^{c,dyn} - P^{c,eq}$ and time derivative of saturation ($\partial S/\partial t$) are known at a given saturation value, τ can be determined.

3 Results and Discussions

3.1 Dynamic Water Saturation Profiles

Figure 1 represents the saturation (S)-time (t) curves for the three samples at 35°C at 50 cm carbon dioxide pressure heads. Although the saturation-time curves are discussed earlier in the context other flow problems, they are important in this study as they are needed to calculate $\partial S/\partial t$ and subsequently the dynamic coefficient. All the simulated curves in this work show that approximately 50% of the water was displaced within seconds of starting the flow (drainage). In the coarse sand sample, approximately 50% of the water was displaced within 5 seconds while the fine sand attained this saturation in less than 180 seconds. The 50% coarse and 50% fine sand mixture attained 50% water saturation within 90 seconds. The time reduced further as the carbon dioxide pressures were increased. Such rapid initial water displacements were most likely due to the high pressures (approximately 15 MPa) imposed on a relatively small domain, measuring only 10 cm in diameter and 12 cm in height.

The importance of the dS/dt curves and their implications are discussed earlier (e.g., Hassanizadeh et al., 2002; Das and Mirzaei, 2012) and is not discussed in detail in this paper. However it must be stated that in consistent with our previous studies (e.g., Das and Mirzaei, 2012), we calculate the dS/dt as shown below,

$$\left. \frac{dS}{dt} \right|_{t_n} = \frac{S|_{t_{n+1}} - S|_{t_{n-1}}}{t_{n+1} - t_{n-1}} \quad (18)$$

where, $S|_{t_{n-1}}$, $S|_{t_n}$ and $S|_{t_{n+1}}$ are the average wetting phase saturation at times t_{n-1} , t_n and t_{n+1} . In general, the rate of change of saturation (dS/dt) changes with saturation and time and, this determines when two-phase flow system reaches capillary equilibrium. As expected, the dS/dt values were the highest at wetting phase saturation values close to 1. The rate falls with the decrease in saturation and was the least at irreducible saturation. For example, $\partial S/\partial t$ values for coarse sand at 35°C and

pressure head of 50 cm ranged between $-2.389 \times 10^{-1} \text{ s}^{-1}$ at 0.9 wetting phase saturation and $-7.222 \times 10^{-7} \text{ s}^{-1}$ at 0.1 wetting phase saturation. Similar trends are observed for fine and mixed sands. It is noteworthy from the results that at low wetting phase saturations, it becomes increasingly difficult to displace water as the domain approaches irreducible saturation. This explains why the time derivatives of saturation for all samples were the highest at wetting phase saturation values close to unity. It also explains the dramatic rise in capillary pressures as water saturation values fall from 0.3 close to irreducible saturation. Similar trends were reported for silicone oil-water system in fine sand (Das et al., 2012a, b) where the desaturation rate was smaller than in the coarse sand sample. It should also be noted that the dS/dt values are related to the mobility ratios, which depend on the relative permeabilities of the fluid phases and the fluid viscosity ratios (Das et al., 2007). In other words, if the mobility ratios change, then dS/dt and, hence, the dynamic coefficient may also change.

In this work we did not find significant effect of temperature on $\partial S/\partial t$ values at high water saturations for all the porous samples. However, the $\partial S/\partial t$ values at low saturations displayed small increases as temperature was increased. In addition, the coarse sand simulation at a temperature of 35°C and CO_2 pressure head of 50 cm readily achieved the irreducible saturation value of 0.0757 within a simulated time of 26 hours. Due to the fine sand sample having the lowest permeability value, irreducible saturation was never achieved at the same time. So, a simulation time of 300 hours on a personal computer (Intel i3 Core, DELL INSPIRON N5040) was required in order to achieve a final saturation value of 0.0778. The mixed sand sample with an intermediate permeability value took 180 hours to attain a final saturation of 0.0758. The simulation times reduced as the carbon dioxide injection pressures were increased, while temperature appeared to have no significant effect on the time taken to achieve irreducible saturation.

3.2 Dynamic and Quasi-Static Capillary Pressure-Saturation Curves

Figures 2 (a-d) represent the dynamic and quasi-static capillary pressure (P^c)-saturation (S) curves for coarse grained sand at 35°C , 45°C , 55°C and 65°C , respectively. In consistent with the trends in the literature, the quasi-static curves lie below the dynamic curves in the figures. This means that at the quasi-static condition, the same saturation is attained at a lower capillary pressure with the dynamic condition and as such, it is important to differentiate between a quasi-static condition and dynamic condition. Also, as the carbon dioxide pressure heads increase, so does the capillary pressures. This can be observed more clearly at the wetting phase saturations below 0.4. It was observed that the distinction between the curves decreased as temperatures were increased. One point of note in this regard is that all P^c -S curves in Figure 2 are calculated using P^c data from all directions (e.g., axial and radial directions). Whether the P^c -S relationships would vary depending on the directions, and if so, how significant these variations would be, are not investigated in this paper.

It should be noted that the dynamic capillary pressure effect is given by the extent of the dependence of $p_c^{c,dyn} - p_c^{c,equ}$ on $\partial S/\partial t$, and not simply $p_c^{c,dyn} - p_c^{c,equ}$. Therefore, although some curves in Figures 2-4 may almost overlap, it does not mean that dynamic capillary pressure effect is not significant in these cases. These points are discussed further in section 3.3.

Findings in this work show that moderate increase in P_c is needed to drain the domain close to irreducible saturation while dramatic capillary pressure rise is often encountered as the system approaches irreducible water saturation. In line with this, Figure 2 shows that relatively low capillary pressure increases were required to reduce water saturations from its initial value of 1.0 to a lower saturation of around 0.3. Further reduction in water saturations closer to the irreducible saturation requires large capillary pressure increases. For example, at a temperature of 35°C and carbon dioxide pressure head of 50 cm, wetting phase saturation of 0.3 was achieved at a capillary pressure of 131 Pa, while residual saturation was achieved at a capillary pressure of 3888 Pa (approximately).

It is also evident that the capillary pressures at irreducible saturation, at higher temperature, were lower than those at 35°C because irreducible saturation increased from 0.0757 to 0.2071 as the domain temperatures were increased from 35°C to 65°C. The closeness of the capillary pressure-saturation curves at higher temperatures can be due to change in viscosity and density at high pressure of supercritical CO₂. Gases at high pressure were reported to undergo rapid change in density resulting in large increase in viscosity (Viswanath, 2007). Figures 3(a-d) represent the dynamic and quasi-static capillary pressure-saturation curves for fine sand at 35°C, 45°C, 55°C and 65°C, respectively. Figures 4 (a-d) represent the dynamic and quasi-static capillary pressure-saturation curves for mixed sand simulations at 35°C, 45°C, 55°C and 65°C, respectively. The trends in these figures are similar to those observed for coarse sand (Figure 2) and are not discussed in length. Figure 5 compares the quasi-static curves for the three porous samples at 35°C. It clearly shows how the capillary pressures tend to vary at various saturations for the three samples with different permeability values. In this case, capillary pressure values at high wetting phase saturations were between those calculated for coarse sand and fine sand. This is because the mixed sand had a permeability value of $5.95 \times 10^{-11} \text{ m}^2$ which is an intermediary between those determined for fine and coarse samples.

3.3 Dynamic Capillary Pressure Effect

The origin of the dynamic capillary pressure effect has been discussed in the introduction of the paper and is avoided here. As mentioned earlier, the dynamic capillary pressure effect, indicated by the dynamic coefficient (τ), was determined from the simulation results of all the porous samples over a range of saturations. Figure 6 shows a semi-log plot of the dynamic coefficient in coarse sand under various simulation conditions. It shows that at all the temperatures, dynamic coefficient values decreased as the wetting phase saturation increased and the values increased dramatically as the

wetting phase saturation declined towards the irreducible value. This has been the general experience in most publications (Hasanizadeh et al., 2002; Manthey et al., 2005; Das and Mirzaei, 2012; Sakaki et al., 2010; Hanspal and Das, 2012) and it is said to be indicative of how far the process is away from equilibrium (Das et al., 2007). As discussed by Das et al. (2007), at high wetting phase saturations, the two fluid phases are well connected, thus shorter times are required for equilibrium to be attained. As the wetting phase saturations decrease, and more supercritical carbon dioxide continuously enters the pore spaces, the remaining water tend to disconnect. In such cases, the dynamic coefficient may be non-monotonic in behaviour (Das et al., 2007; Mirzaei and Das, 2007). Similar behaviour is found in this work.

As visible from Figure 6, the dynamic coefficient at higher temperatures overlies the lower temperature ones at the same saturation point with the exception for simulations at high saturation (>0.75) and 65°C where the starting point lies slightly below the values of τ at 55°C . Also, the dynamic coefficient at 45°C shows fluctuations throughout the entire saturation profile but the average effect overlies the τ values at lower temperature, i.e., 35°C . This is similar to the experience of Hanspal and Das (2012) who noted the increase in τ values as the temperature rises. The fluctuations experienced were most likely due to the high pressures (approximately 15 MPa) imposed on a domain measuring only 10 cm in diameter and 12 cm in height. Variation in saturation distribution of supercritical CO_2 may arise from temperature dependency of its density and viscosity. This may result in the change of the mobility ratios of the two fluid phases present in the domain. However, these are not studied in this paper. At water saturation of 0.1, τ value of 8.73×10^8 Pa.s was calculated for coarse domain at 35°C . From Figure 6, the general trend is the rising τ values as the temperature increases. But, because the simulations at high temperature could not be conducted for low saturation values as irreducible saturation increases with temperature, it is difficult to estimate the τ values at these points. However, it can be inferred that the τ values at saturation close to or less than 0.1, for higher temperatures will be higher than the value at 35°C .

In comparison, Hanspal and Das (2012) reported the highest τ values of 5.33×10^8 Pa.s at 80°C and 9.1×10^6 Pa.s at 20°C in coarse sand of closely comparable properties at saturation points of 0.33 and 0.191, respectively. This is a slightly lower τ value in our case (8.73×10^8 Pa.s) at 35°C , though it is noteworthy that the final saturation values of estimations in their publication were well above 0.1. Bottero et al. (2011b), in their experiment on tetrachloroethylene-water system, reported average values for dynamic coefficient, at the scale length of 11cm, in the range of 0.5×10^6 Pa.s and 1.2×10^6 Pa.s. These are upscaled values of the dynamic coefficients and were found to have increased by one order of magnitude than the local-scale coefficients (1.3×10^5 to 2×10^5 Pa.s). Furthermore, their upscaled values at scale length of 18 cm were 1.5×10^6 and 2.5×10^6 Pa.s. Juxtaposing these values

with our results, especially at 11 cm scale which correspond to the domain size in our simulation, it is clear that the dynamic effects in CO₂-water system is more significant.

Similarly, the values of τ for the CO₂-H₂O system in this work maintain a large gap from the values reported by Das and Mirzaei (2012) in their work on silicone oil-water system. The same domain size was used while the fine and coarse sand samples used in their work were of comparable properties to the ones used in this work. They reported the highest average values less than 1×10^6 and 8×10^5 Pa.s for fine and coarse sand samples, respectively. So, it can again be inferred that supercritical CO₂ undergoes pore scale processes which raise the dynamism of the CO₂-H₂O-sand system to a higher degree than the silicone oil-water and tetrachloroethylene-water systems.

Figure 7 shows that the fluctuating patterns experienced under coarse sand for one or two conditions are more pronounced in fine sand. This could be attributed to low permeability of the fine sand sample. Again, changes in temperature dependent density and viscosity ratios coupled with the domain properties are responsible for this observation. Calculated dynamic coefficient values in the fine sand are significantly higher than those determined for coarse sand, with a value as high as 8.10×10^9 Pa.s calculated at a temperature of 35°C and wetting phase saturation of 0.1. This implies that it would take much longer to attain capillary equilibrium in porous media with lower permeability values.

As expected, the mixed porous sample had dynamic coefficient values between those reported for coarse and fine grained sand samples. This is due to the fact that the mixed sand has a permeability value lower than coarse sand but higher than fine sand. In this case, τ values as high as 6.02×10^9 Pa.s were found as shown in Figure 8. A comparison of the dynamic effects in the three different sand samples is shown in Figure 9. It is visible that the effect has the highest magnitude in the fine sand. This trend is consistent with observations in previous studies (e.g., Das and Mirzaei, 2012, 2013).

The effects of the boundary conditions were also investigated on τ values and the results are shown in Figure 10. In general, the dynamic coefficient is known to vary slightly as the boundary conditions; however some authors have shown no or negligible effects of boundary conditions (Camps-Roach et al., 2010). The extent of this change is not known for the system under investigation. As explained before, four different dynamic boundary pressures were used to determine τ so far. To investigate the effects of the imposed pressure, 50, 70, 100 and 135 cm CO₂ heads were used in one set of simulation (Table 8) and 150, 200, 250 and 300 cm are used as a new set of boundary conditions. In both of these cases, the boundary condition at the bottom of the domain and initial pressure for water are as stated in Table 8 for 35°C (308.15K). For the new set of boundary condition we have carried out the required simulations to calculate the dynamic coefficient which are presented in Figure 10. From the figure, it can be seen that the τ values at different imposed pressure sets are mostly similar at the

same wetting phase saturation, see for example, the τ values at water saturations of 0.1 and 0.9. All τ values for the two sets of boundary pressures could not be obtained at exactly the same water saturations, and, therefore, they should be compared carefully; however, we can reasonably infer that the different sets of boundary conditions exhibit similar trend at similar water saturations. However, as the imposed pressure is increase, the dynamic coefficient may be increased slightly at the same temperature. In this work, results from the first set of boundary pressures were reported. One further point that should be noted is that although the exact saturation for a typical CO₂ plume may vary from case to case depending on a number of issues, the results in this work (Figures 6 – 10) show that the dynamic effect is significantly increased from a fully saturated domain as the saturation decreases, particularly at lower water saturation (<40%).

We have also investigated the effects of grid size on the values of the dynamic coefficient, so as to confirm the reliability of the results. Two different grid sizes were chosen and their effects on the dynamic coefficient (τ) were then determined. The grids used for this purpose included 40 and 416 nodes for the same domain (i.e., 3D cylindrical domain measuring 10 cm in diameter and 12 cm in height). Of the grids the one with 416 nodes is the grid that was used to generate the results presented in this paper so far. The other grid involved a case where the number of nodes was decreased approximately 10 folds. The numerical simulations were then carried out for a typical case, namely, coarse domain at 35°C for the same boundary conditions (Table 8). Quasi-static and dynamic capillary pressure curves were generated for the additional two cases which were then used to determine the dynamic coefficients for the respective cases. Closeness was observed in the τ values obtained under the different grid densities and it provides the confidence that the grid size does not have significant effect on the numerical results in this paper. Similar conclusion for grid size effect was obtained by others earlier (Das et al, 2004; Das et al, 2007; Hanspal and Das, 2012).

4. Conclusions

Well defined numerical simulations to determine dynamic and quasi-static P^c-S relationships have been conducted for a supercritical carbon dioxide-water flow in homogeneous core scale porous samples. Much like other reported studies on two-phase flow in porous media, the P^c-S relationships in CO₂-H₂O-sand system follow a regular pattern with increasing capillary pressure as the water saturation decreases. The results also show that the dynamic and quasi-static P^c-S relationships do not vary significantly for the fluid properties at a particular temperature. However, they depend on S and time derivative of saturation ($\partial S/\partial t$), and as such, it can be concluded that the dynamic capillary pressure effect is an important factor to consider. We have used three dynamic P^c-S curves (corresponding to three different dynamic pressure heads) and one quasi-static P^c-S curve to determine an average value of τ at a particular saturation. The results in this work suggest that the time to capillary equilibrium during geological sequestration of CO₂ should be accounted for while simulating the flow processes, e.g., to determine the CO₂ storage capacity of a geological aquifer. To

simulate the field scale processes, one would require both the fundamental understanding of the dynamic capillary pressure effects for supercritical CO₂-water flow in terms of P^c-S relationship as well as the knowledge on how significant the τ values are for these cases. These are addressed in this paper. The approach used in this work to determine the τ values should be viewed as an 'inverse approach' where all the necessary process variables are assumed known except the values of the dynamic coefficient. As its values are determined in this paper, a 'forward problem' for simulating the dynamic CO₂-H₂O flow which couples the dynamic capillary pressure equation with traditional two-phase flow modelling approaches can be set up. To apply the results of this work in the field setting, one would need to upscale these core scale results to field scale.

The most significant contribution of this work is that it provides a fundamental understanding of the significance of dynamic capillary pressure effect for supercritical CO₂-water flow in porous media. For example, the dynamic coefficients determined in this work reflect a higher value than some contemporary reports for oil-water system in the literatures under comparable conditions. It is shown that the flow of CO₂-H₂O is affected by the factors of fluid and media properties. Under similar conditions, increasing τ values of 8.73×10^8 Pa.s, 6.02×10^9 Pa.s and 8.1×10^9 Pa.s were respectively calculated in coarse, mixed and fine grained sand samples whose permeabilities were 3.65×10^{-10} m², 5.95×10^{-11} m² and 5.66×10^{-11} m², respectively. This indicates that the system experiences more gap away from equilibrium as the media permeability decreases. This similar effect reflects in the simulation times required to attain irreducible saturation in the various porous media as the time increases with decreasing permeability. The results further show that τ increases with temperature and may increase slightly at higher flow rate/pressure at the same pressure.

As we have explained in the paper, there are some studies which have simulated CO₂-water flow in porous media without the consideration of dynamic effects which may introduce some errors in the modelling calculations. When one does not consider these effects (i.e., $\tau = 0$), it effectively implies that dynamic and quasi-static P^c-S relationships are the same. However, our results show that $\tau \neq 0$ and it varies as a function of saturation. The results suggest that at large water saturation, the τ values are small. In other words there would be smaller errors in the modelling calculations if one chose to use a traditional modelling scheme based on quasi-static P^c relation (i.e., equation 1). As the water saturation decreases, the τ values increase. In other words, the errors in the calculation are likely to increase should one chose to use equation (1) to account for the capillary pressures in the modelling calculations. The key point here is that any error calculations should really be done for a range of saturations as the error estimate is likely to be saturation dependent. It also needs a 'forward problem' as discussed in the paper so that a typical modelling solution may be compared for a range of dynamic coefficients. Such an approach has been tried by Fučík et al (2010) and Peszyńska and Yi (2009) for a two-phase flow problem (i.e., not CO₂-water flow); but, these authors have assumed that

τ is independent of saturation. A detailed study on error estimates for flow of CO₂-water flow in porous media for the cases when the dynamic coefficient is saturation dependent should be tried in the future.

5. References

Abidoeye, L.K., Das, D.B., Khudaida, K, 2014. Geological Carbon Sequestration in the Context of Two-Phase Flow in Porous Media: A Review. *Critical Reviews in Environmental Science and Technology*, DOI: 10.1080/10643389.2014.924184 (in press).

Bennion D.B., and Bachu S, 2006. Supercritical CO₂ and H₂S–brine drainage and imbibition relative permeability relationships for intergranular sandstone and carbonate formations. Paper presented in SPE Europec/EAGE annual conference and exhibition, Vienna, Austria, 12–15 June.

Bachu, S. and Bennion, D.B., 2009. Dependence of CO₂-brine Interfacial Tension on Aquifer Pressure, Temperature and Water Salinity. *Energy Procedia*, **1**, 3157-3164.

Benson, S.M., Li, B., Krause, M., Krevor, S., Kuo, C., and Pini, R., 2011. Investigations in Geologic Carbon Sequestration: Multiphase Flow of CO₂ and water in reservoir rocks. Department of Energy Resources Engineering, School of Earth Sciences, Stanford University, **1**, 19-20.

Birkholzer, J.T., Zhou, Q., and Tsang, C., 2009. Large-scale impact of CO₂ storage in deep saline aquifers: A sensitivity study on pressure response in stratified systems. *International Journal of Greenhouse Gas Control*, **3**, 181-194.

Bottero, S., Hassanizadeh, S.M., Kleingeld, P.J., 2011(a). From Local Measurement to an Upscaled Capillary Pressure-Saturation Curve. *Trans Porous Med* (2011) **88**:271-291.

Bottero, S., Hassanizadeh, S.M., Kleingeld, P.J., and Heimovaara, T.J., 2011(b). Nonequilibrium capillarity effects in two-phase flow through porous media at different scales. *Water Resources Research* **47**, W10505, doi: 10.1029/2011WR010887, 2011.

Brooks RH, Corey A, 1964. Hydraulic Properties of Porous Media. *Hydrology Papers*. Fort Collins, CO: Colorado State University.

Camps-Roach, G., O'Carroll, D.M., Newson, T.A., Sakaki, T., Illangasekare, T.H.: Experimental investigation of dynamic effects in capillary pressure: grain size dependency and upscaling. *Water Resources Research*, 46(8), 1-13 (2010)

Cheol Huh, Seong-Gil Kang, Sup Hong, Jong-Su Choi, Jong-Hwa Baek, Chul-Soo Lee, Yong-Chan Park, Jung-Suk Lee, (2009). CO₂ storage in marine geological structure: A review of latest progress and its application in Korea. *Energy Procedia*, 1, 3993–4000

Chin-Fu Tsang, Jens Birkholzer, Jonny Rutqvist, 2008.. A comparative review of hydrologic issues involved in geologic storage of CO₂ and injection disposal of liquid waste. *Environ Geol.* 54:1723–1737, DOI 10.1007/s00254-007-0949-6

Chiquet, P., Daridon, J., Broseta, D., and Thibeau, S., 2007. CO₂/water interfacial tensions under pressure and temperature conditions of CO₂ geological storage. *Energy Conversion and Management*, 48, 736-744.

Christine Doughty and Karsten Pruess, 2003. Modelling Supercritical Co₂ Injection in Heterogenous Porous Media. Proceedings, TOUGH Symposium, California, May 12-14.

Civan, F., 2012. Temperature Dependency of Dynamic Coefficient for Nonequilibrium Capillary Pressure-Saturation Relationships. *American Institute of Chemical Engineers*, 58 (7), 2282-2285.

Civan, F. (2007). Critical Modification to the Vogel-Tammann-Fulcher Equation for Temperature Effect on the Density of Water. *Industrial Engineering and Chemistry Research Journal*, **46** (17), 5810 -5814.

Daneshfar, J., Hughes, R.G., and Civan, F. (2009). Feasibility Investigation and Modeling Analysis of CO₂ Sequestration in Arbuckle Formation Utilizing Salt Water Disposal Wells. *Journal of Energy Resources Technology*, 131(2), Article Number: 023301, pp. 1-10.

Das, D., Gaudie, R., and Mirzaei, M., 2007. Dynamic Effects for Two-Phase Flow in Porous Media: Fluid Property Effects. *American Institute of Chemical Engineers*, 53(10), 2505-2520.

Das, DB, Mirzaei, M. 2012. Dynamic effects in capillary pressure relationships for two-phase flow in porous media: Experiments and Numerical Analyses. *AIChE Journal*, 58(6), 1951- 1965, DOI: 10.1002/aic.12702

Das, DB and Mirzaei, M. (2013). Experimental measurement of dynamic effect in capillary pressure relationship for two-phase flow in weakly layered porous media. *AIChE Journal*, 59(5), 1723–1734.

Dahle, H.K., Celia, M.A., Hassanizadeh, S.M., 2005. Bundle-of-tubes model for calculating dynamic effects in the capillary-pressure-saturation relationship. *Transport Porous Media* **58**, 5-22.

Ennis-King, J., and L. Paterson, 2003. Role of Convective Mixing in the Long-Term Storage of Carbon Dioxide in Deep Saline Formations, paper SPE-84344, presented at Society of Petroleum Engineers Annual Fall Technical Conference and Exhibition, Denver, CO, October

Fenghour, A., Wakeham, W.A., and Vesovic, V., 1998. The Viscosity of Carbon Dioxide. *Journal of Physical and Chemical Reference Data*, 27, 31-44.

Fučík, R., Mikyška, J., Sakaki, T., Beneš, M., Illangasekare TH. 2010. Significance of Dynamic Effect in Capillarity during Drainage Experiments in Layered Porous Media, *Vadose Zone J.* 9:697–708, doi:09.0106/vzj2009.0106.

Jeremy Camps-Roach, Denis M. O'Carroll, Timothy A. Newson, Toshihiro Sakaki and Tissa H. Illangasekare, 2010. Experimental Investigation of Dynamic Effects in Capillary Pressure: Grain Size Dependency and Upscaling. *Water Resources Research*, 46, W08544.

Goal, G and O'Carroll, DM, 2011. Experimental investigation of nonequilibrium capillarity effects: Fluid viscosity effects. *Water Resources Research*, VOL. 47, W09507, doi:10.1029/2010WR009861, 2011

Hanspal, N and Das, DB, 2012. Dynamic Effects on Capillary Pressure-Saturation Relationships for Two-Phase Porous Flow: Implications of Temperature. *AIChE Journal*, 58(6), 1951-1965, DOI: 10.1002/aic.12702.

Hanspal N, Allison B, Deka L, Das DB. (2013). Artificial neural network (ANN) modeling of dynamic effects on two-phase flow in homogeneous porous media. *J Hydroinformatics*, 15(2), 540–554 doi:10.2166/hydro.2012.119.

Hassanizadeh SM, Gray WG, 1990. Mechanics and thermodynamics of multiphase flow in porous media including interphase boundaries. *Adv Water Resour.* 13:169–186

Hassanizadeh, S.M., Gray, W.G., 1993. Thermodynamic basic of capillary pressure in porous media. *Water Resources Research* 29 (10), 3389-3405.

Hassanizadeh, S.M., Celia, M.A., Dahle, H.K., 2002. Dynamic effect in the capillary pressure-saturation relationship and its impact on unsaturated flow. *Agricultural Sciences* 7(2), 69-71.

Juanes, R, 2008. Nonequilibrium effects in models of three-phase flow in porous media. *Advances in Water Resources* 31 (2008) 661–673.

Kalaydjian, F (1992). Effect of the Flow Rate on an Imbibition Capillary Pressure Curve-Theory Versus Experiment. In SCA European Core Analysis Symposium, Institute Francais du Petrole, Rueil-Malmaison, France, 175-194.

Khudaida. K. J. and Das, D.B. 2014. A numerical study of capillary pressure–saturation relationship for supercritical carbon dioxide (CO₂) injection in deep saline aquifer. Chemical Engineering Research and Design, DOI: 10.1016/j.cherd.2014.04.020 (in press).

Lopez, O., Idowu, N., Rueslatten, H., Boassen, T., Leary, S., and Ringrose, P., 2011. Pore-scale modelling of CO₂-brine flow properties at In Salah, Algeria. Energy Procedia, **4**, 3762-3769.

Mazen M. Abu-Khader. Recent Progress in CO₂ Capture/Sequestration: A Review. Energy Sources, Part A, 28:1261–1279, 2006. DOI: 10.1080/009083190933825

Meyer CA, McIntock RB, Silvestri GJ, Spencer RC. ASME Steam Tables: Thermodynamic and Transport for Steam and Water. 6th Ed. 1967:13–30, American Society of Mechanical Engineers, New York.

Michael, K., Golab, A., Shulakova, V., Ennis-King, J., Allinson, G., Sharma, S., and Aiken, T., 2010. Geological Storage of CO₂ in Saline Aquifers – A Review of the Experience from Existing Storage Operations. International Journal of Greenhouse Gas Control, **4**, 659-667.

Mirzaei, M., Das, D.B., 2007. Dynamic effects in capillary pressure saturations relationships for two-phase flow in 3D porous media: Implications of micro-heterogeneities. Chemical Engineering Science 62, 1927-1947.

Mirzaei, M., Das, D.B., 2013. Experimental investigation of hysteretic dynamic effect in capillary pressure–saturation relationship for two-phase flow in porous media. AIChE Journal, 59(10), 3958–3974, DOI: 10.1002/aic.14121.

Nadja Müller, 2011. Supercritical CO₂-Brine Relative Permeability Experiments in Reservoir Rocks—Literature Review and Recommendations. Transp Porous Med, 87:367–383 DOI 10.1007/s11242-010-9689-2

Nordbotten, J.M., Celia, M.A., Bachu, S., 2004. Injection and Storage of CO₂ in Deep Saline Aquifers: Analytical Solution for CO₂ Plume Evolution During Injection. Transport in Porous Media, **58**, 339-343.

Nordbotten, J.M., Celia, M.A., Dahle, H.K., and Hassanizadeh, S.M. 2008. On the definition of macro-scale pressure for multi-phase flow in porous media. *Water Resources Research* 44(6), W06S02, doi: 10.1029/2006WR005715.

Nordbotten, J.M., Celia, M.A., Dahle, H.K., and Hassanizadeh, S.M. 2007. Interpretation of macroscale variables in Darcy's law. *Water Resources Research* 43: W08430. doi: 10.1029/2006WR005018.

Nordbotten, J. M., J. P. Nogues, and M. A. Celia. 2010, Appropriate Choice of Average Pressure for Upscaling Relative Permeability in Dynamic Flow Conditions, *SPE*, 228-237.

Ozgun, E. and Gumrah, F., 2009. Diffusive and Convective Mechanisms during CO₂ Sequestration in Aquifers. *Energy Sources, Part A: Recovery, Utilization and Environmental Effects*, **31 (8)**, 698-709.

Peszyńska, M and Yi, S-Y. 2008. Numerical Method for unsaturated flow with dynamic capillary pressure in heterogeneous porous media. *International Journal of Numerical Analysis and Modeling*, Volume 5, Supp, Pages 126-149.

Paul Zakkour, Mike Haines, 2007. Permitting issues for CO₂ capture, transport and geological storage: A review of Europe, USA, Canada and Australia. *International journal of greenhouse gas control*, 1, 94 – 100

Perrin, J., Krause, M., Kuo, C., Miljkovic, L., Charoba, E., and Benson, S., 2009. Core-scale experimental study of relative permeability properties of CO₂ and brine in reservoir rocks. *Energy Procedia*, **1**, 3515-3522.

Plug, W., and Bruining, J., 2007. Capillary pressure for the sand-CO₂-water system under various pressure conditions. Application to CO₂ sequestration. *Advances in Water Resources*, **30**, 2339-2353.

Pruess, K., and K. Zhang, 2008, Numerical Modeling Studies of the Dissolution-Diffusion-Convective Process during CO₂ Storage in Saline Aquifers, Paper LBNL-1243E, Lawrence Berkeley National Laboratory, Berkeley, Calif.,

Riaz, A., H. A. Tchelepi, and F. M. Orr, 2006. Onset of Convection in a Gravitationally Unstable Diffusive Boundary Layer in Porous Media, *Journal of Fluid Mechanics*, 548:87–111.

Sakaki, T, O'Carroll, DM, Illangasekare, TH., 2010. Direct Quantification of Dynamic Effects in Capillary Pressure for Drainage-Wetting Cycles. *Vadose Zone Journal*, 9(2): 424-437.

Sally M. Benson and David R. Cole, 2008. CO₂ Sequestration in Deep Sedimentary Formations. Elements, Vol. 4, pp.325-331.

Shukla, R., Ranjith, P., Haque, A. and Choi, X., 2010. A review of studies on CO₂ sequestration and caprock integrity. Fuel, 89, 2651-2664.

Stanmore , B.R., and Gilot, P. 2005. Review - Calcination and Carbonation of Limestone During Thermal Cycling For CO₂ Sequestration. Fuel Processing technology 86 (2005): 1707-1743.

Viswanath, D.S., Ghosh, T.K., Prasad, D.H.L., Dutt, N.V.K., Rani, K.Y. 2007. Viscosity of Liquids: Theory, Estimation, Experiment, and Data. Dordrecht, The Netherlands. Springer, ISBN-10 1-4020-5481-5(HB). (p 113).

White, M.D., and Oostrom, M., 2006. STOMP, Subsurface Transport Over Multiple Phases, Version 4.0, User's Guide. Pacific Northwest National Laboratory, pp.13,14, 63-93.

Zahid, U., Lim, Y., Jung, J. and Han, C., 2011. CO₂ geological storage: A review on present and future prospects. Korean Journal of Chemical Engineering, 28 (3), 674-685.

Table 1. Carbon dioxide and water densities for various temperatures at 15 MPa Pressure

Temperature (K)	308.15	318.15	328.15	338.15
Carbon dioxide Density (kg m ⁻³)	815	735	645	535
Water Density (kg m ⁻³)	994	990	986	980

Table 2. Liquid Water Constants for Equation (10) (Hanspal and Das, 2012)

A_{11}	7.98E+00	a_1	8.44E-01
A_{12}	-2.62E02	a_2	5.36E-04
A_{13}	1.52E-03	a_3	1.72E+00
A_{14}	2.28E-02	a_4	7.34E-02
A_{15}	2.42E+02	a_5	4.98E-02
A_{16}	1.27E-10	a_6	6.54E-01
A_{17}	2.07E-07	a_7	1.15E-06
A_{18}	2.17E-08	a_8	1.51E-05
A_{19}	1.11E-09	a_9	1.42E-01
A_{20}	1.29E+01	a_{10}	7.00E+00
A_{21}	1.31E-05	a_{11}	3.00E-04
A_{22}	6.05E-14	a_{12}	2.04E-01

Table 3. Supercritical Carbon Dioxide and Water Viscosities for various Temperatures at 15 MPa Pressure

Temperature (K)	308.15	318.15	328.15	338.15
Carbon dioxide Viscosity (10^{-5} Pa s)	7.2	6.2	5.0	4.2
Water Viscosity (10^{-4} Pa s)	7.4	6.1	5.2	4.4

Table 4. Supercritical Carbon Dioxide-Water and Air-Water Interfacial Tensions at different Temperatures

Temperature, K	308.15	318.15	328.15	338.15
Carbon dioxide-Water Interfacial Tension (dyn cm ⁻¹)	18.1	21.3	27.2	31.3
Water-Air Interfacial Tension (dyn cm ⁻¹)	70.4	68.8	67.1	65.4

Table 5. Irreducible water Saturation at Different Temperature

Temperature (K)	308.15	318.15	328.15	338.15
Irreducible Saturation (-)	0.0757	0.1195	0.1633	0.2071

Table 6. Experimentally Measured Physical Properties of the Porous Media that were used in the Numerical Simulations in this work

Material Properties	Coarse Sand	Fine Sand	50% Coarse and 50% Fine Sand Mixture
Permeability, K (m^2)	3.65×10^{-10}	5.66×10^{-11}	5.95×10^{-11}
Particle Density, ρ ($kg\ m^{-3}$)	2740	2660	2700
Porosity, Φ (-)	0.37	0.38	0.34
Pore Size Distribution Index, λ (-)	3.86	2.49	3.18
Entry Pressure, P^d ($N\ m^{-2}$)	370	1325	848

Table 7. Geometry of 3D Cylindrical Domain, showing the Number of Nodes and Nodal Spacing

Number of Nodes x Nodal Spacing		
$N \times \Delta r$ (m)	$N \times \Delta \theta$ (degrees)	$N \times \Delta Z$ (m)
4 x 0.01275	4 x 90	1 x 0.0005 24 x 0.005 1 x 0.0005

Table 8. Initial and Boundary Conditions for the Dynamic Simulations

Temperature (K)		308.15	318.15	328.15	338.15
Initial Water Pressure (Pa)		15001144	15001139	15001134	15001128
Top Carbon dioxide Pressure (Pa)	Dynamic 1	15003991	15003599	15003185	15002620
	Dynamic 2	15005587	15005039	15004422	15003668
	Dynamic 3	15007982	15007198	15006317	15005240
	Dynamic 4	15010775	15009718	15008528	15007073
Bottom Water Pressure (Pa)		15001178	15001173	15001168	15001162

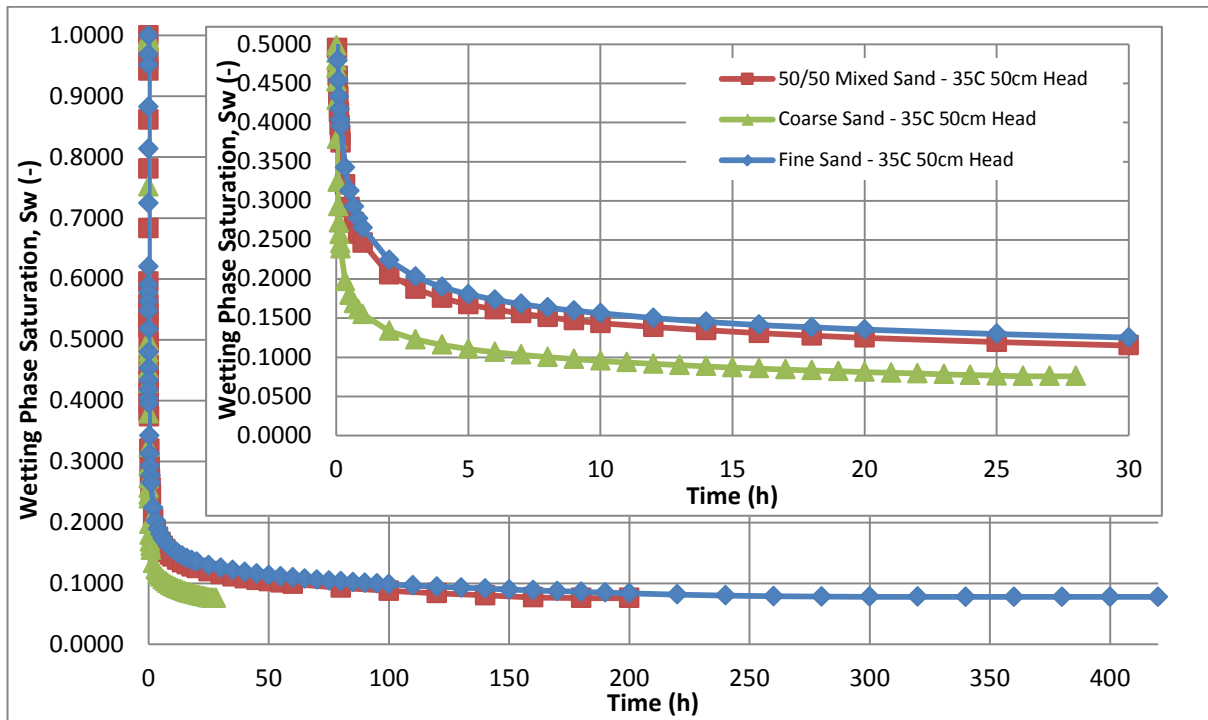
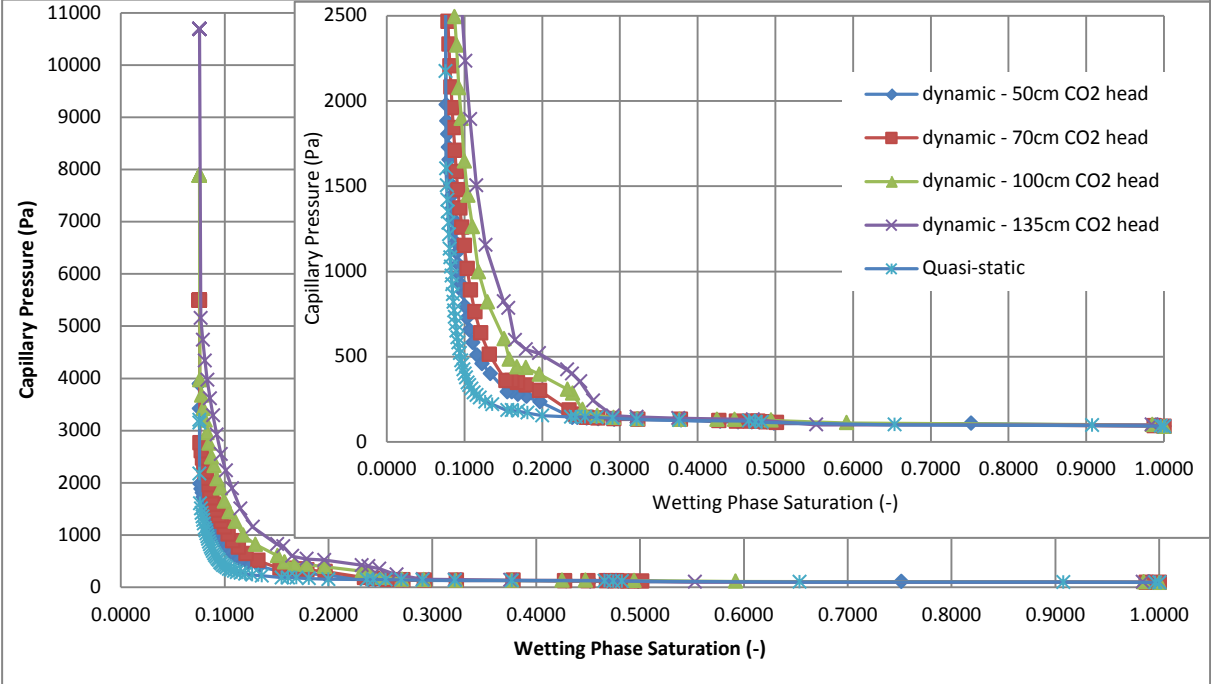
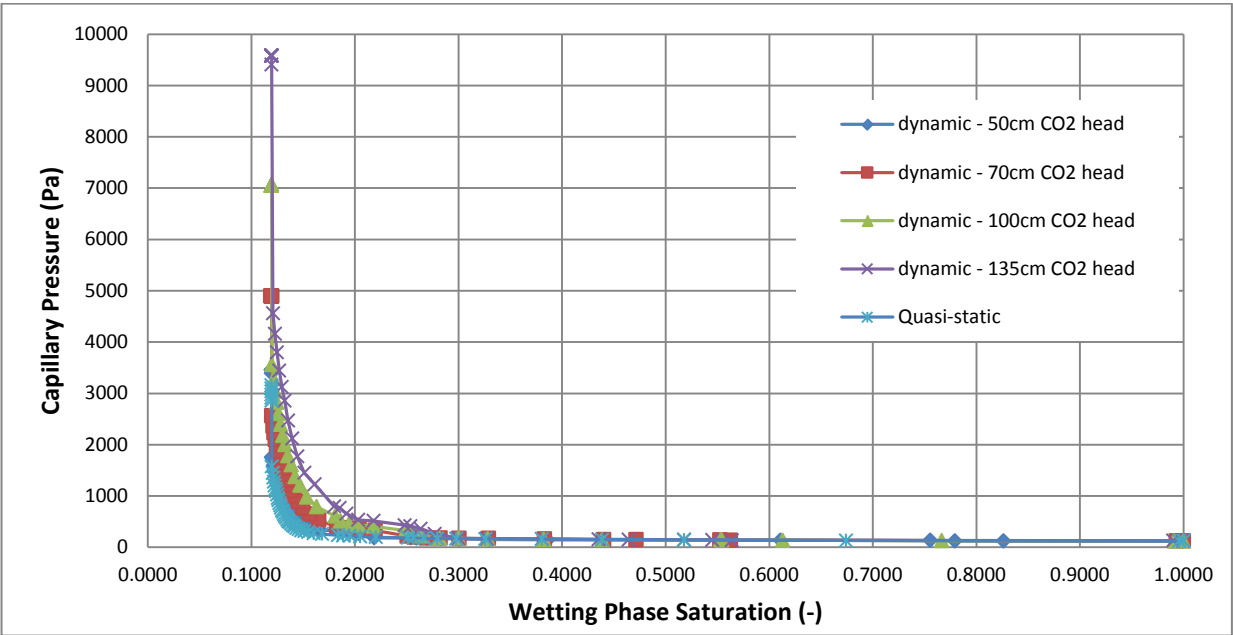


Figure 1. Saturation-Time curves for Coarse Sand, Fine Sand and Mixed Sand, all obtained at 35°C and pressure heads of 50 cm. These curves are based on porous medium properties obtained from experimental measurements (Table 6).

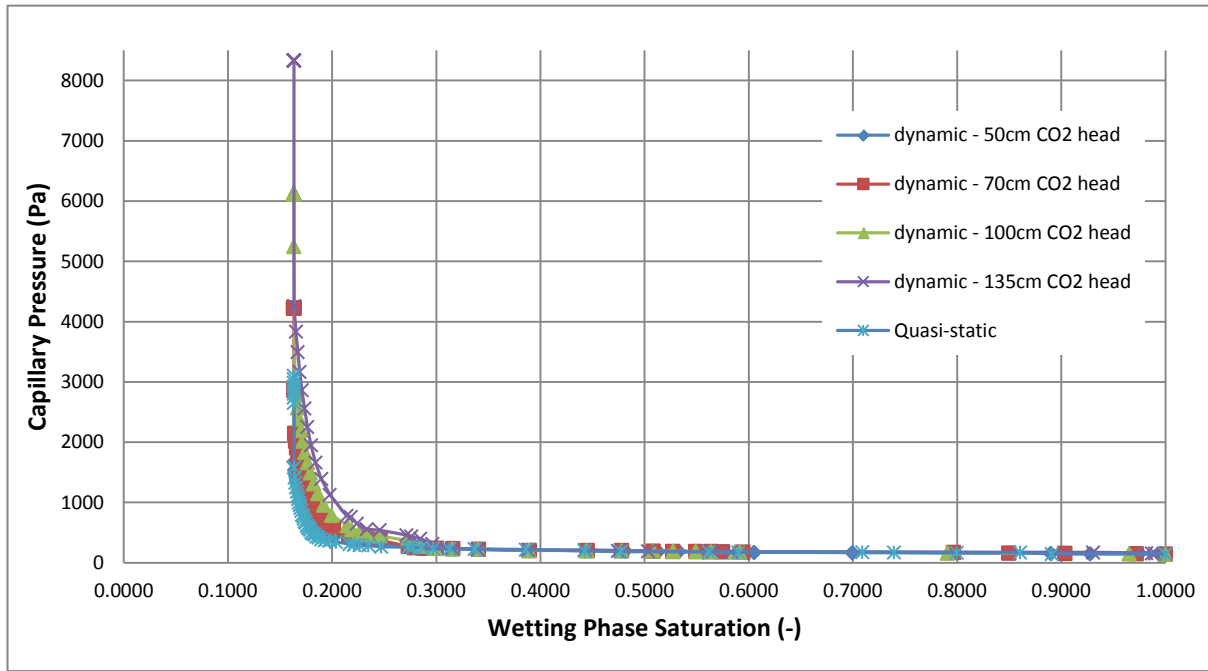
(a)



(b)



(c)



(d)

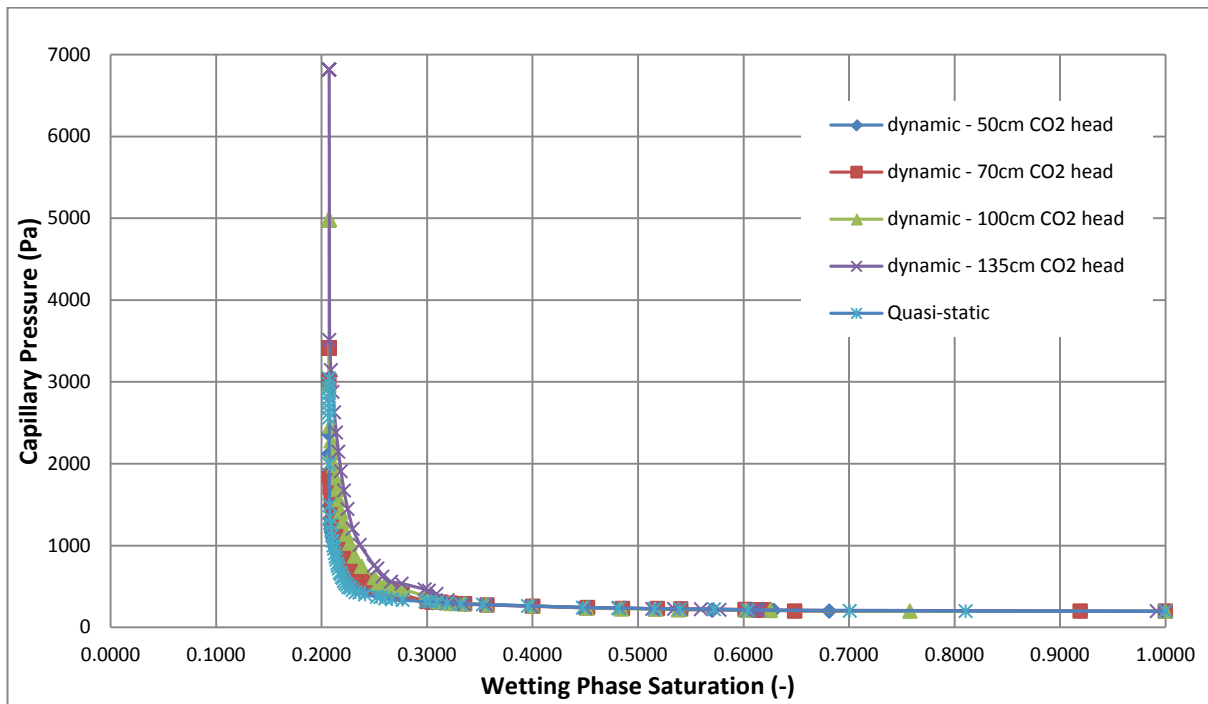
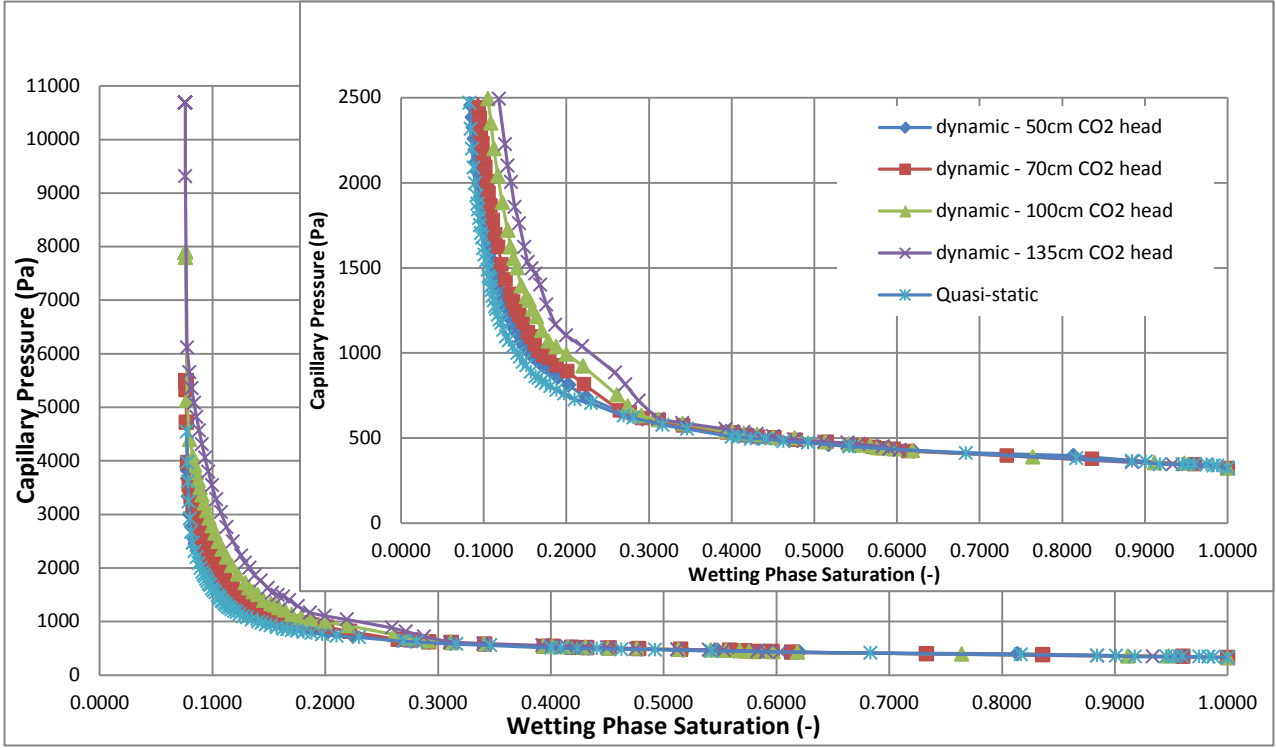
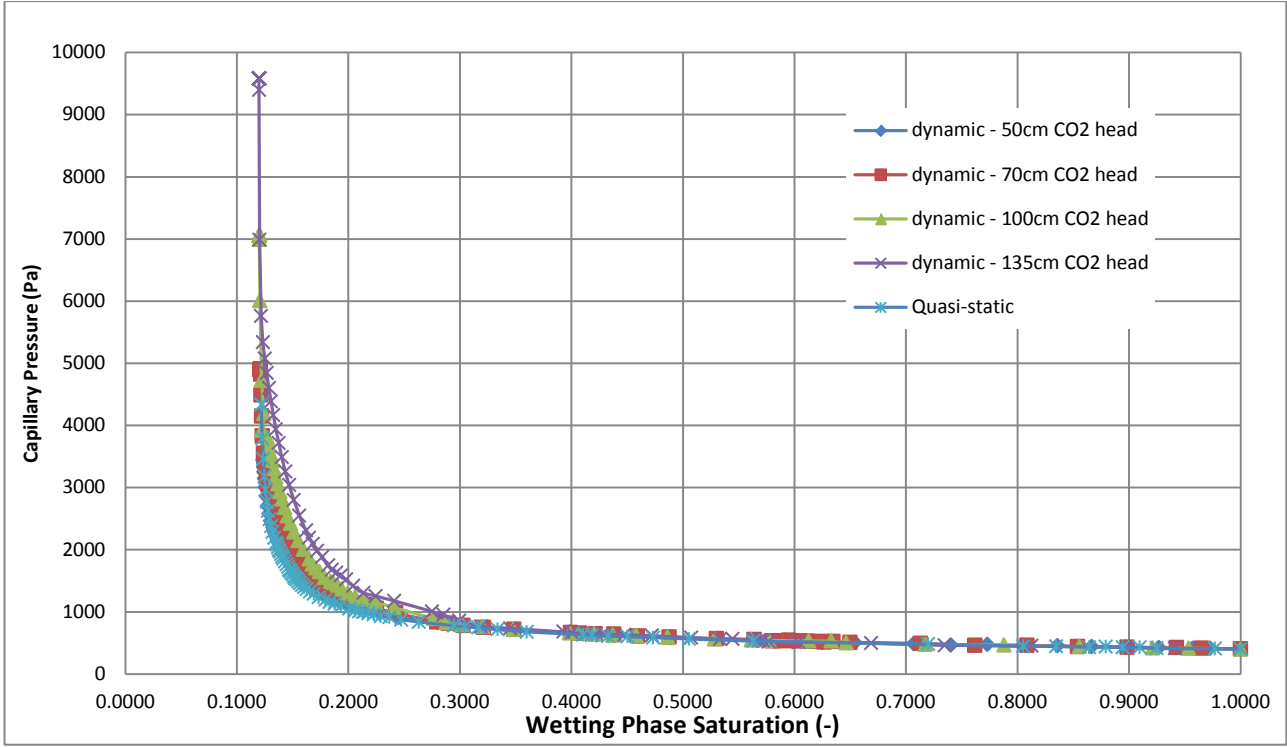


Figure 2. Dynamic and Quasi-Static Capillary Pressure – Saturation Curves for Coarse Sand at (a) 35°C, (b) 45°C, (c) 55°C and (d) 65°C. These curves are based on porous medium properties obtained from experimental measurements (Table 6).

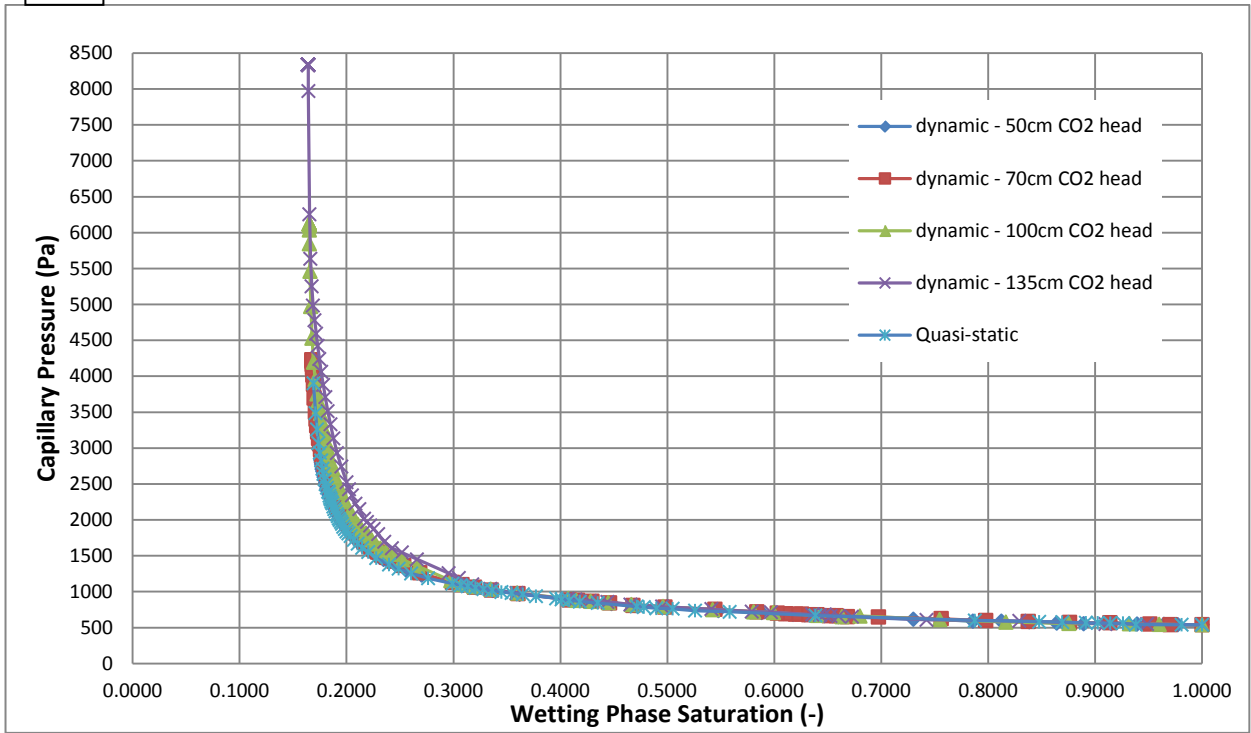
(a)



(b)



(c)



(d)

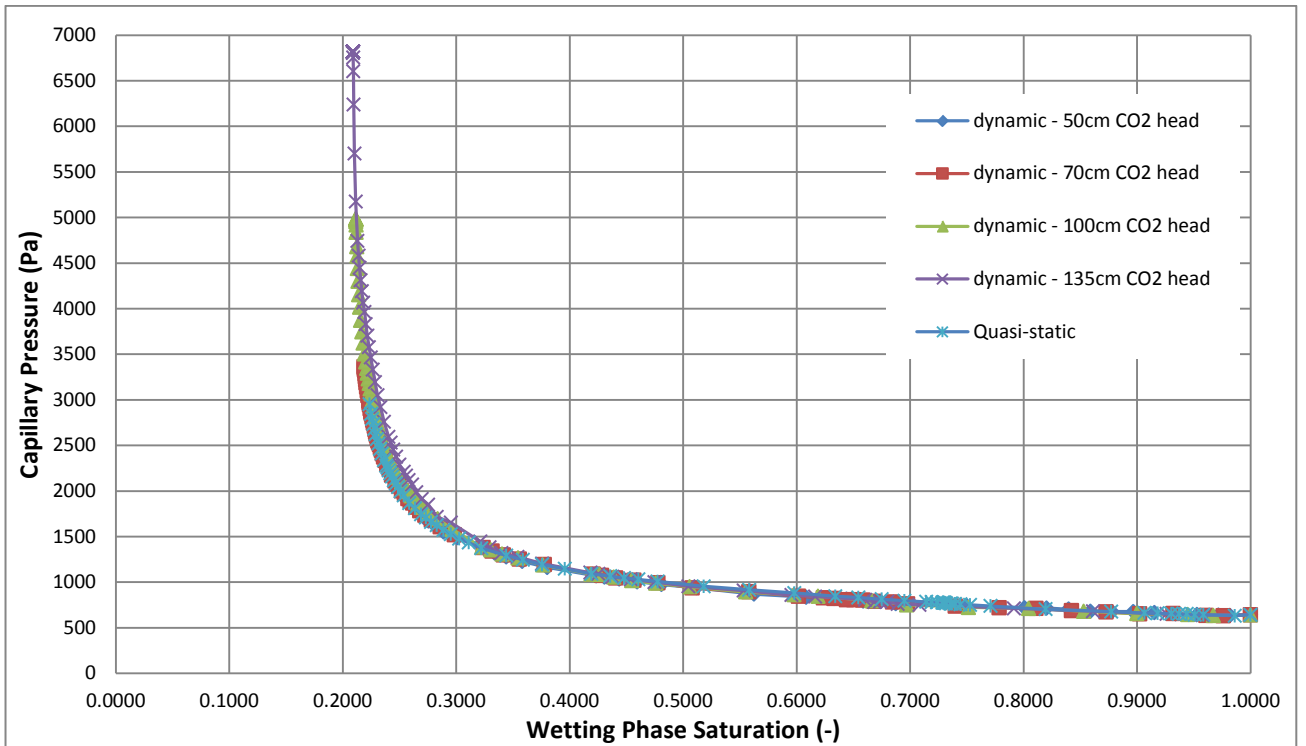
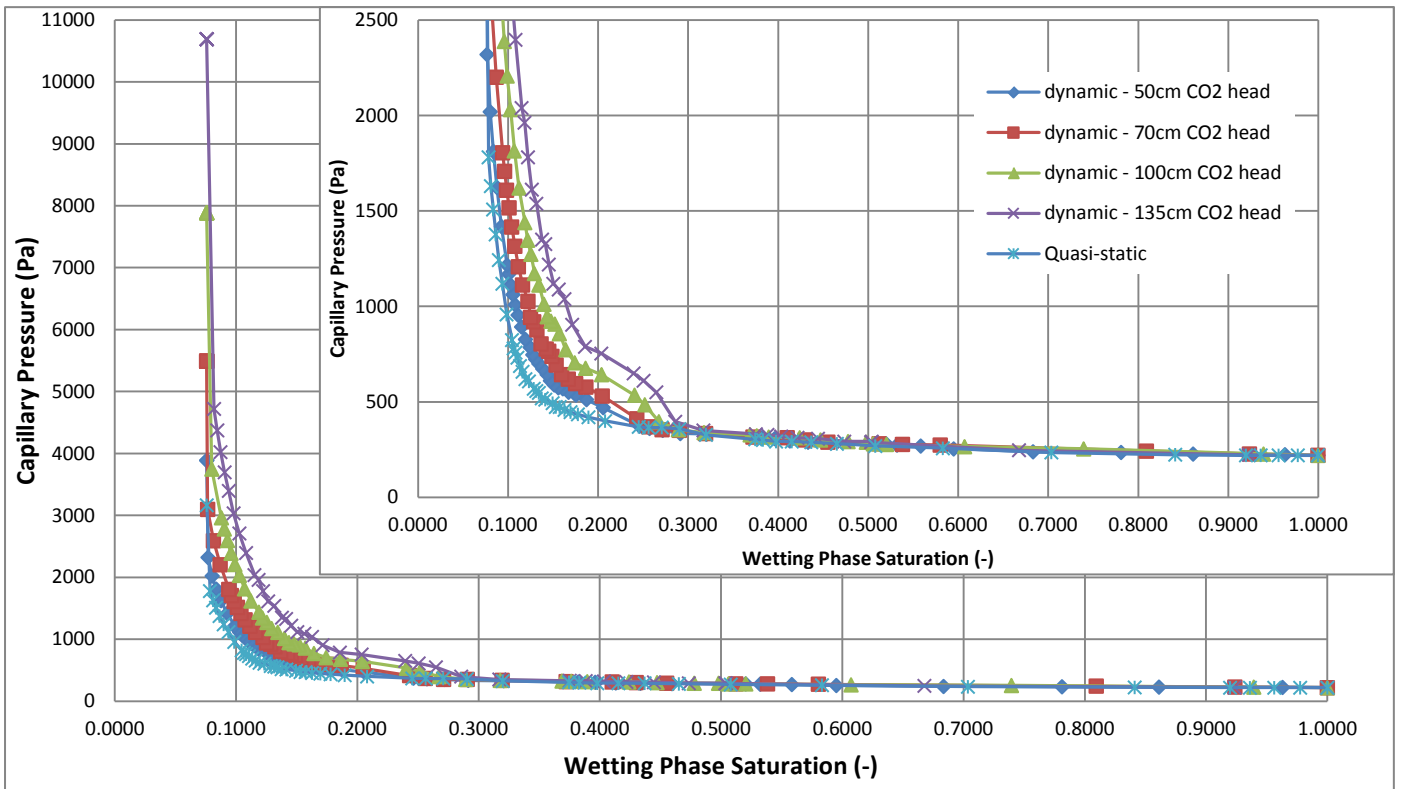
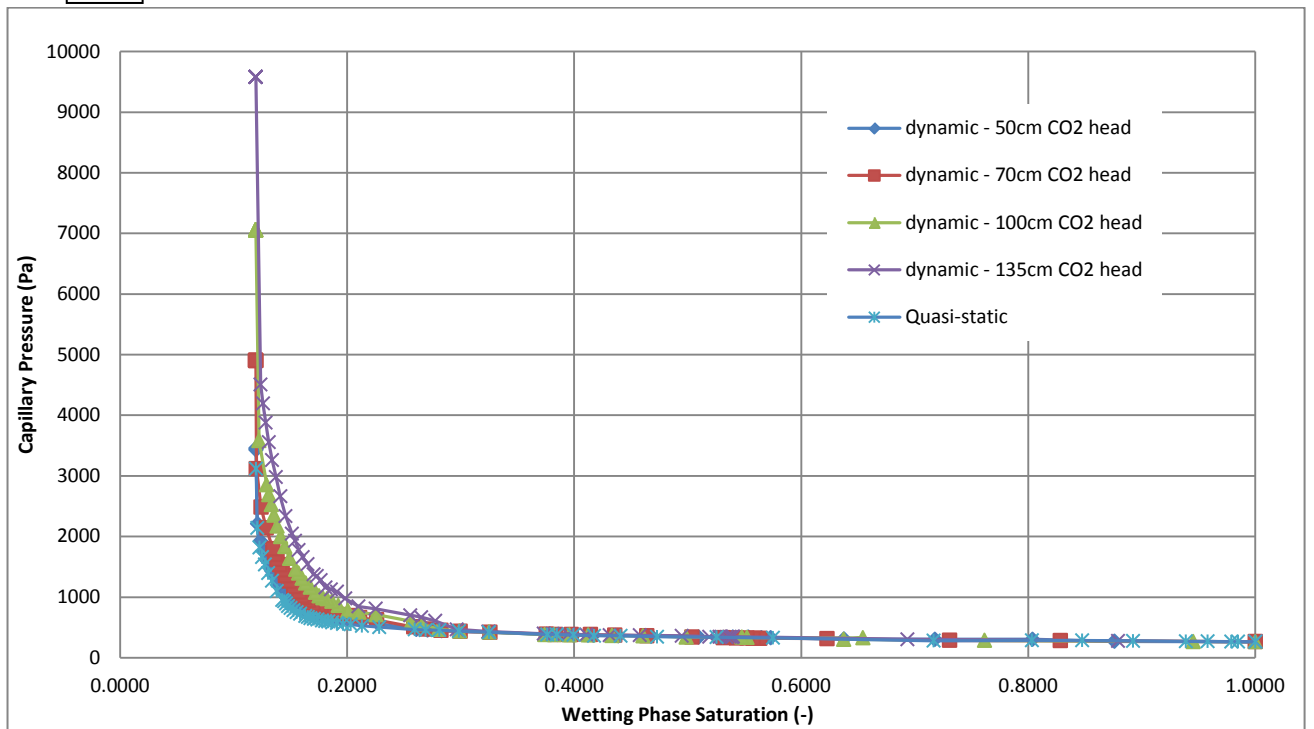


Figure 3. Dynamic and Quasi-Static Capillary Pressure – Saturation Curves for Fine Sand at (a) 35°C, (b) 45°C, (c) 55°C and (d) 65°C. These curves are based on porous medium properties obtained from experimental measurements (Table 6).

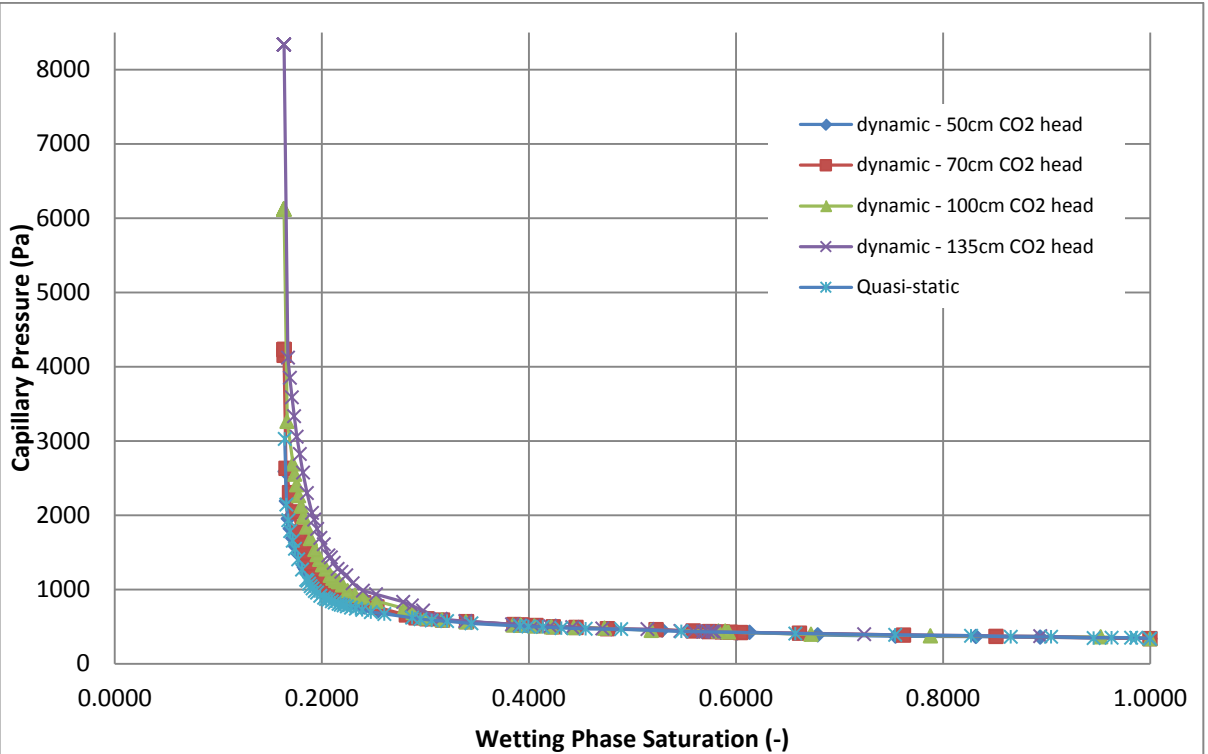
(a)



(b)



(c)



(d)

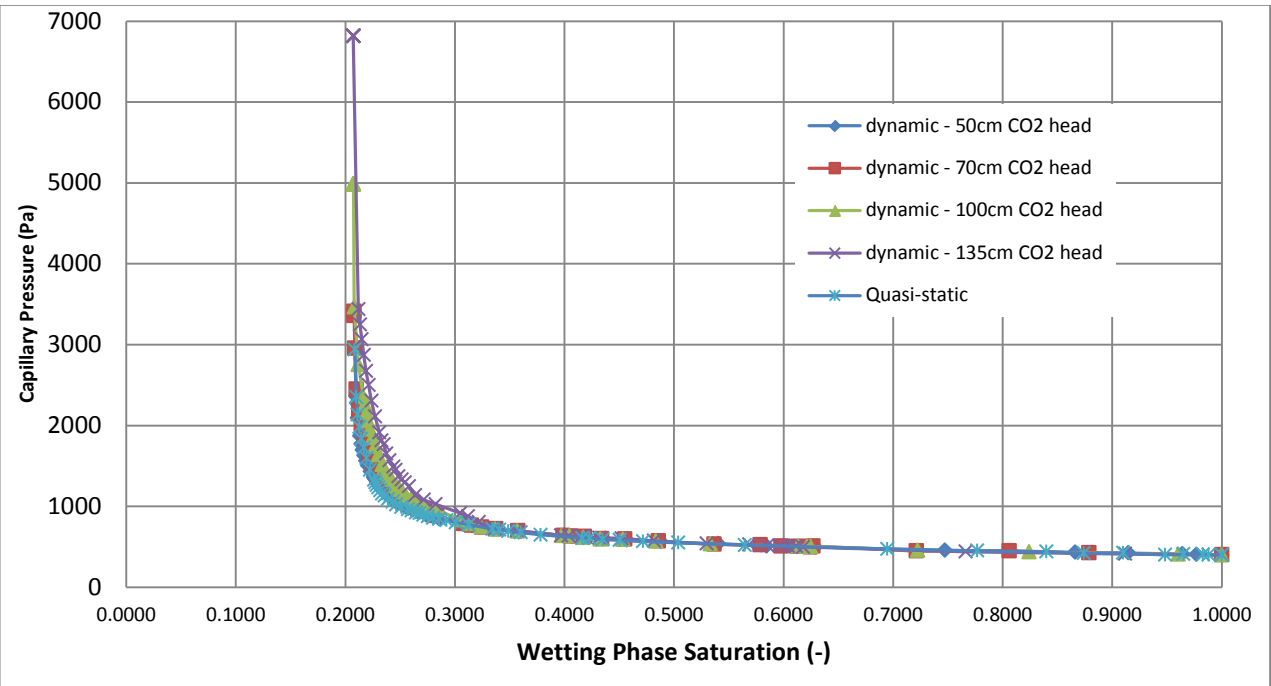


Figure 4. Dynamic and Quasi-Static Capillary Pressure – Saturation Curves for 50% Fine Sand and 50% Coarse Sand Mixture at (a) 35°C, (b) 45°C, (c) 55°C and (d) 65°C. These curves are based on porous medium properties obtained from experimental measurements (Table 6).

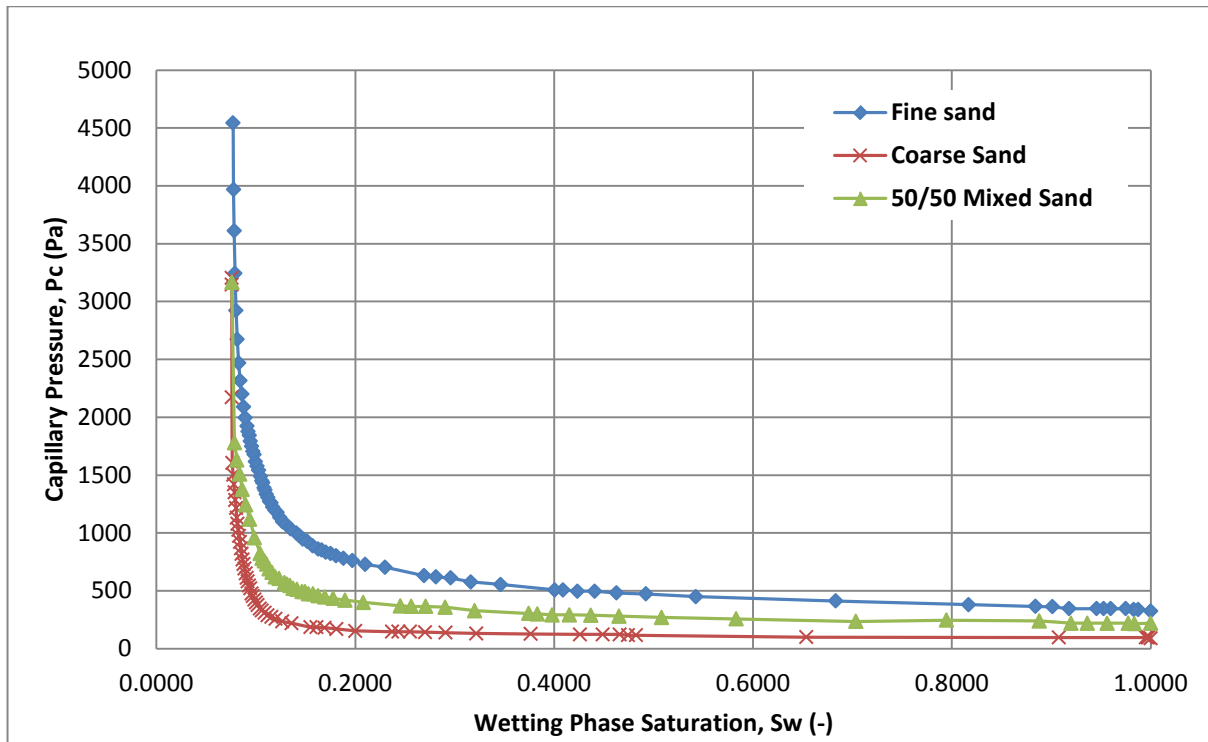


Figure 5. Comparison of Quasi-Static Capillary Pressure–Saturation Curves for Fine Sand, Coarse Sand and 50% Fine Sand and 50% Coarse Sand Mixture at 35⁰C. These curves are based on porous medium properties obtained from experimental measurements (Table 6).

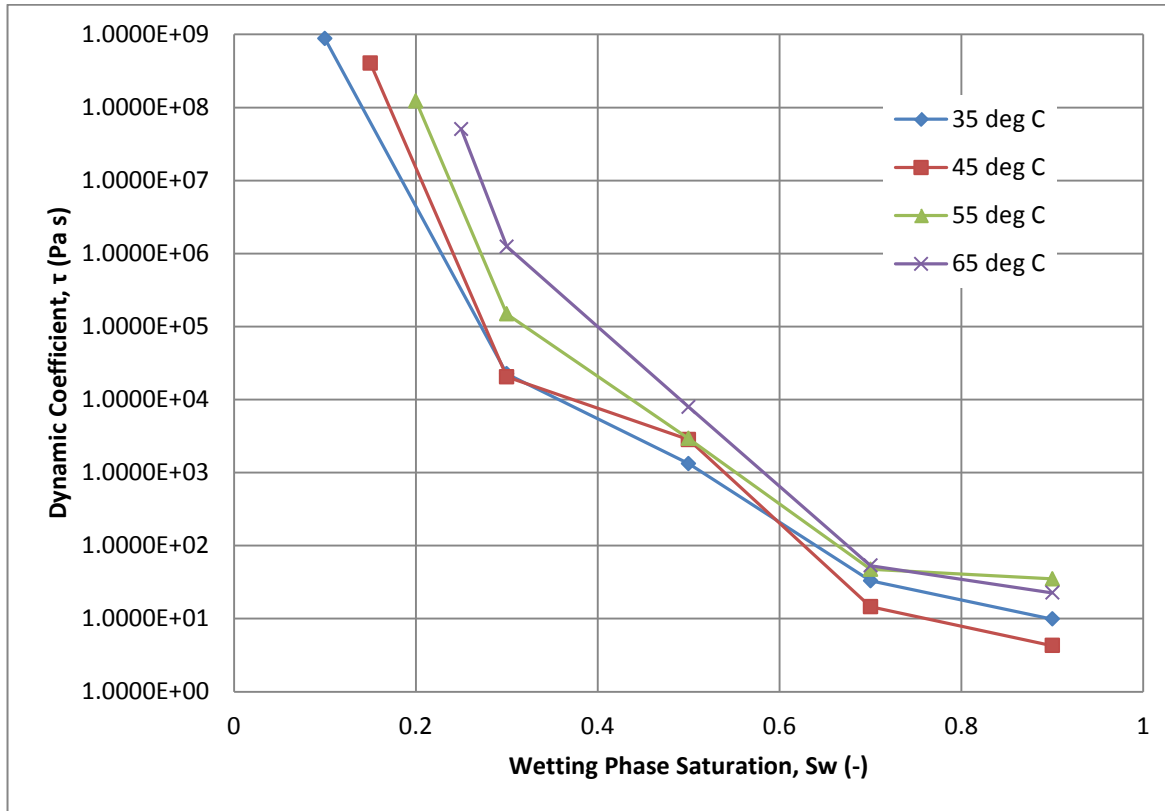


Figure 6: Dynamic Coefficients in Coarse Sand at Different Temperatures. These semi-log plots are based on porous medium properties obtained from experimental measurements (Table 6).

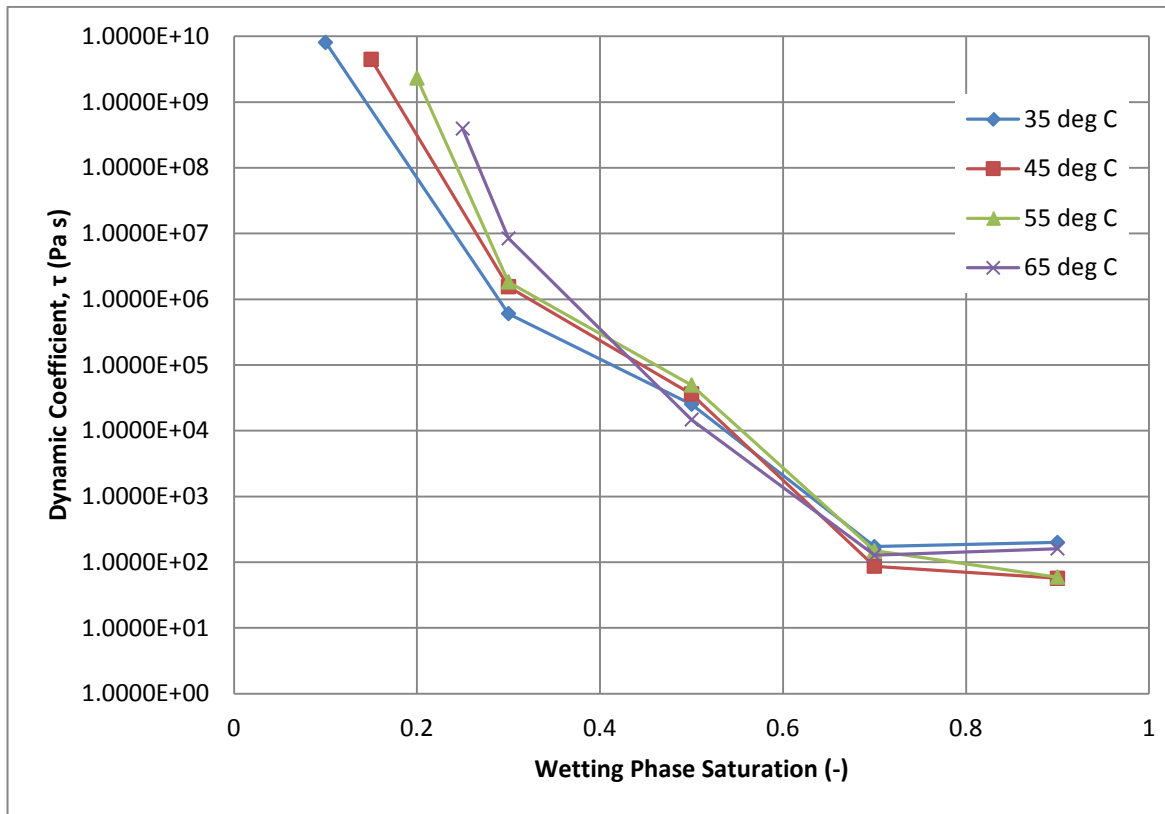


Figure 7: Dynamic Coefficients in Fine Sand at Different Temperatures. These semi-log plots are based on porous medium properties obtained from experimental measurements (Table 6).

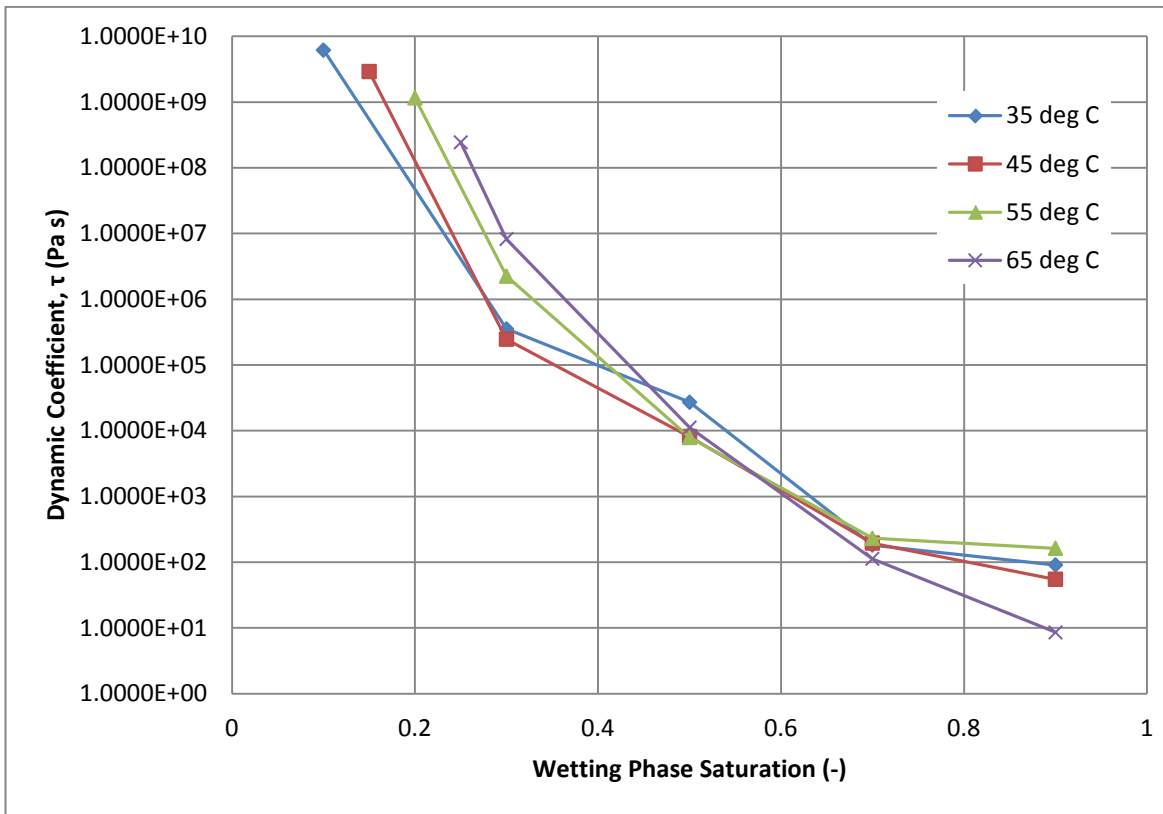


Figure 8: Dynamic Coefficients in Mixed Sand Sample at Different Temperatures. These semi-log plots are based on porous medium properties obtained from experimental measurements (Table 6).

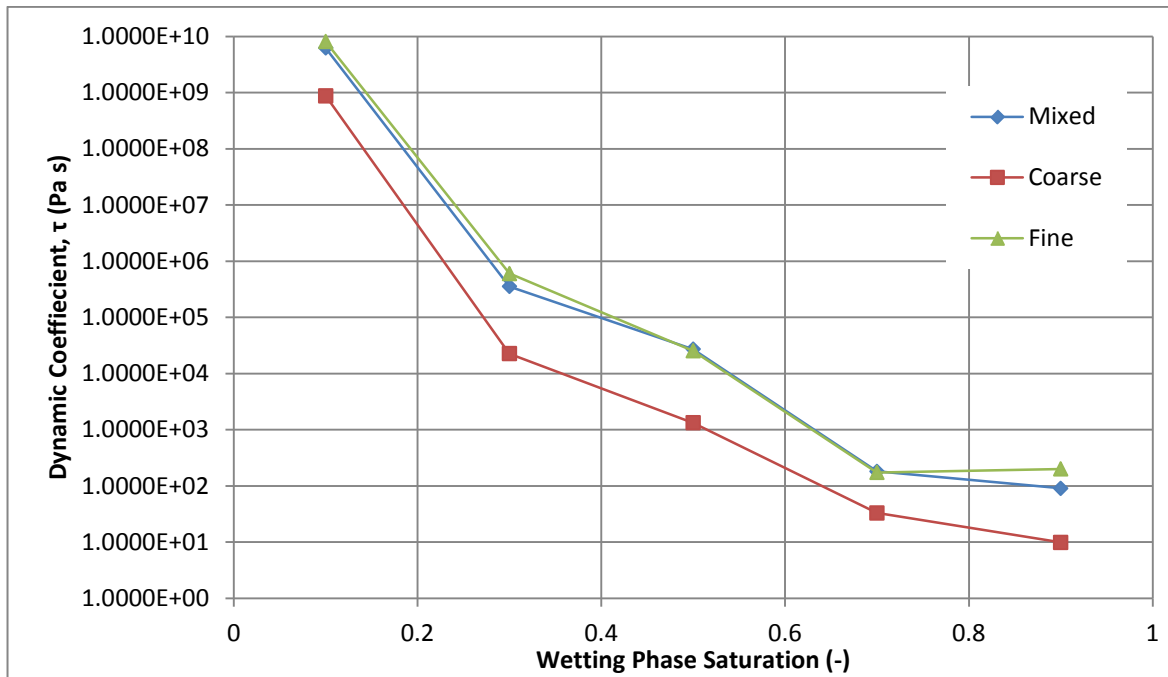


Figure 9: Dynamic Coefficients in Coarse, Fine and Mixed Sand Samples at 35°C. These semi-log plots are based on porous medium properties obtained from experimental measurements (Table 6).

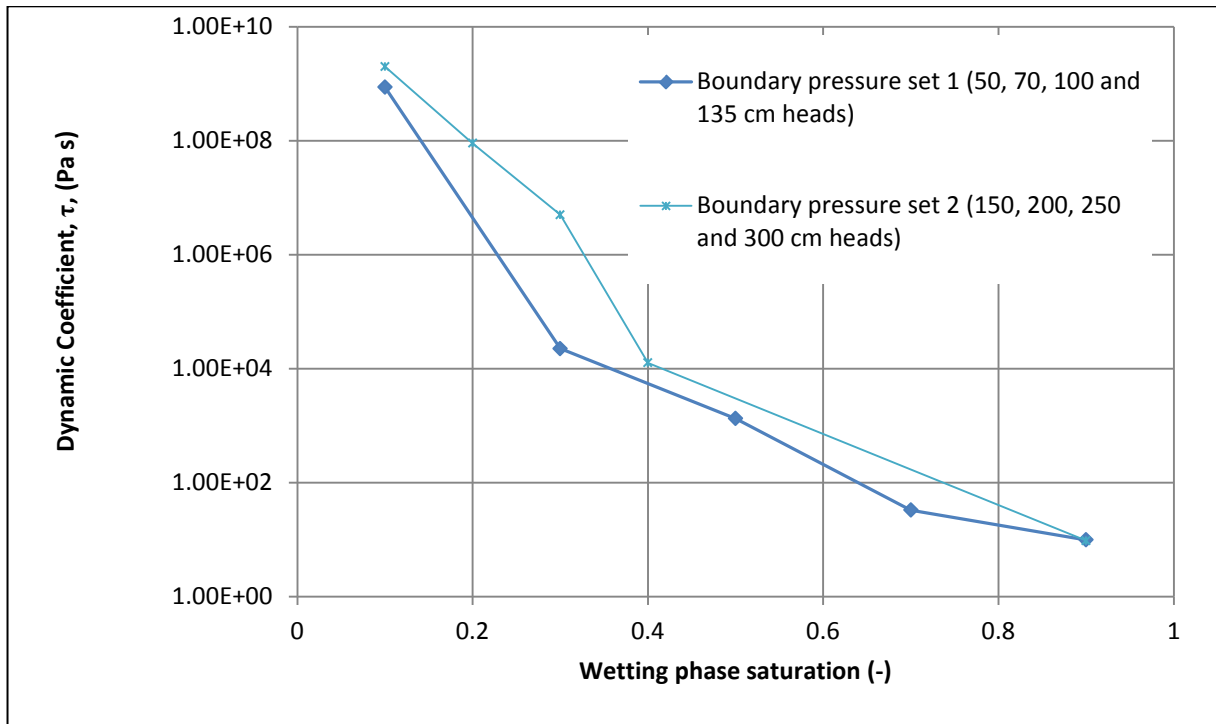


Figure 10: Dynamic coefficients from different set of boundary conditions. Please note that boundary pressure set 1 was applied in all other results in this paper including grid convergence test (Figures 1 – 9). These semi-log plots are based on porous medium properties obtained from experimental measurements (Table 6).